



HAL
open science

Aquifer-CO2 leak project : Physicochemical characterization of the CO2 leakage impact on a carbonate shallow freshwater aquifer

Anélia Petit, Adrian Cerepi, Corinne Loisy, Olivier Le Roux, Léna Rossi, Audrey Estublier, Julien Gance, Bruno Garcia, Benoit Hautefeuille, Bernard Lavielle, et al.

► To cite this version:

Anélia Petit, Adrian Cerepi, Corinne Loisy, Olivier Le Roux, Léna Rossi, et al.. Aquifer-CO2 leak project: Physicochemical characterization of the CO2 leakage impact on a carbonate shallow freshwater aquifer. *International Journal of Greenhouse Gas Control*, 2021, 106, pp.103231. 10.1016/j.ijggc.2020.103231 . hal-03159937

HAL Id: hal-03159937

<https://ifp.hal.science/hal-03159937>

Submitted on 4 Mar 2021

HAL is a multi-disciplinary open access archive for the deposit and dissemination of scientific research documents, whether they are published or not. The documents may come from teaching and research institutions in France or abroad, or from public or private research centers.

L'archive ouverte pluridisciplinaire **HAL**, est destinée au dépôt et à la diffusion de documents scientifiques de niveau recherche, publiés ou non, émanant des établissements d'enseignement et de recherche français ou étrangers, des laboratoires publics ou privés.

Aquifer-CO₂ Leak project: Physicochemical characterization of the CO₂ leakage impact on a carbonate shallow freshwater aquifer

Anélie PETIT^a, Adrian CEREP^a, Corinne LOISY^a, Olivier LE ROUX^a, Léna ROSSI^a,
Audrey ESTUBLIER^b, Julien GANCE^c, Bruno GARCIA^b, Benoit HAUTEFEUILLE^d,
Bernard LAVIELLE^e, Thomas BRICHART^d, Sonia NOIREZ^b, Frédéric MARTIN^b, Benoit
TEXIER^c, Sean KENNEDY^a, Aïcha EL KHAMLICHI^f

^a, EA 4592 Georessources et Environnement, ENSEGID-Bordeaux INP, avenue des Facultés,
33400 Talence, France

^b, IFP Energies nouvelles, 1 & 4 avenue du Bois Preau, 92852 Rueil-Malmaison, France

^c, IRIS Instruments, 1 avenue Buffon, 45100 Orléans, France

^d, GLINCS S.A.S-L'Atrium, 43 boulevard du 11 Novembre 1918, 69100 Villeurbanne, France

^e, CENBG-IN2P3, 19 rue du Solarium, 33170 Gradignan, France

^f, ADEME, 20 avenue du Grésillé, 49000 Angers, France

*e-mail: anelia.petit@ensegid.fr

Abstract

This work is part of the *Aquifer CO₂-Leak project* and aims to understand, quantify and model the environmental impact of a CO₂ leak on water quality in the carbonate freshwater aquifer as well as CO₂-water-carbonate interactions. The experiment has been performed within an Oligocene carbonate underground quarry located in Saint-Emilion (France).

A water charged with dissolved CO₂ was injected in the aquifer through a borehole. Downstream, seven wells were fitted with in-situ probes which automatically measured physicochemical parameters. Periodic water samplings in all wells have been undertaken to determine the elemental concentrations by ion chromatography.

The spread of CO₂ in the groundwater was monitored as a function of time and was observed to influence the various physicochemical parameters. Five parameters seem to be excellent

indicators for monitoring a gas plume during CO₂ geological storage in regard to our results: electrical conductivity and pH, and Ca²⁺, HCO₃⁻, and CO_{2(aq)} concentrations.

The interaction between CO₂ and limestone is highlighted by a saturation index (SI) calculated with PhreeqC software. It shows (i) a slight trend to dissolution of calcite in the injection well (SI<0) linked to the reaction process between CO₂-H₂O-CaCO₃ and (ii) a transport process via diffusion for the observation wells with a SI≈0.

The evolution of physicochemical signatures in the aquifer allows us to understand the reactive and transport processes that occur during the migration of a gasified water plume in the context of leakage from a geological storage reservoir. Our results will make possible to model a leakage in a complex natural reservoir.

Keywords: CO₂ leakage monitoring – Shallow carbonate freshwater aquifer - CO₂-rock-water interactions – Field experiment – CO₂ geological storage

1. Introduction

Since the pre-industrial era, carbon dioxide (CO₂) concentrations have continually increased, with a notable growth of more than 70% (IPCC, 2014). This gas is one of the primary causes of global warming (Albritton and Meira Filho, 2001), mainly related to human activities (fossil fuel consumption, industrial processes, bioenergy, etc.; e.g., IPCC, 1997; Roberts et al., 2018). Carbon Capture and Storage (CCS) is one of the solutions proposed to significantly reduce CO₂ emissions (IPCC, 2005; Bachu, 2008). This is thanks to geological sequestration (e.g. Holloway, 1997a and 1997b; Gale, 2004; Hepple and Benson, 2005) which can be done in aquifers in three phases: trapping of residual gases, trapping by solubility and trapping by mineralization (Roberts et al., 2018). The CO₂ injection is occurring in saline reservoirs that are overlain by freshwater aquifers. These latter must imperatively be protected against a potential leak of CO₂ because of their direct link with human activity (Lee et al., 2016).

Assessing the impacts of CO₂ leakage on shallow aquifers has only received significant attention over the last ten years, Myers et al. (2018) have determined how tracers (CH₄ in this case) can be used to identify and quantify a rate of CO₂ leakage in an aqueous environment through benchtop experiments. Recently, Ju et al. (2020) carried out a CO₂ injection experiment in a shallow aquifer. They used the tracers of noble gases to follow its migration and determine the mass balance of the plume that leaked (especially with Kr having the highest signal).

One of the projects addressing these different issues is the multidisciplinary research project *ZERT* (Zero Emission Research and Technology), which has given rise to numerous publications (Ambats et al., 2009; Strazisar et al., 2009; Kharaka et al., 2010; Oldenburg et al., 2010; Zheng et al., 2012). To do this, 300 kg/day of food-grade CO₂ was injected between July 9 to August 7, 2008 into a horizontal perforated pipe placed below the water table in Bozeman,

Montana (Zheng et al., 2012). The main objective of this project was to assess monitoring techniques (via the detection, location and quantification of potential CO₂ leaks) of geological CO₂ storage sites. Different aspects helping to understand the CO₂ migration pathways were studied. Kharaka et al. (2010) studied the chemical changes linked to the CO₂ injection on the quality of groundwater, via the quantification of major, minor and trace inorganic and organic compounds. The latter evaluated the detection of a CO₂ leak, based in particular on measurements of pH, alkalinity, electrical conductivity. The authors have thus shown that pH is an excellent early indicator of the intrusion of CO₂ into the aquifer.

Other sites have also studied the physicochemical impact of CO₂ injection. For example, the Frio pilot site (operated by the Bureau of Economic Geology of the University of Texas), where a small volume of CO₂ (1600 t) was injected at 1500 m into a brine containing sandstone (Hovorka et al., 2006). Among other things, the changes in pH and alkalinity values observed have been attributed to carbonates dissolution (Kharaka et al., 2006). The Weyburn oil field (Saskatchewan, Canada), corresponds to the first large CO₂-EOR injection project where Encana Corporation introduces 5000 t/day of CO₂ since 2000 (Gaus, 2010). This project studies variations in pH and bicarbonates by carbonate dissolution. The CO₂ injection site in Nagaoka (Japan) operated by the Research Institute of Innovative Technology for the Earth, shows that one year after stopping the injection, high levels of bicarbonate and calcium were still recorded (Gaus, 2010). At Sleipner site (North Sea, Norway, operated by Statoil), 1 Mt of CO₂ per year has been injected into a deep aquifer since 1996 (Holloway et al., 2007). According to this same authors, time-lapse seismic surveys show that no leakage from the storage reservoir has taken place. Lindeberg and Bergmo (2003) explain that the absence of leak is linked to the dissolution of CO₂ into the surrounding pore waters which is more important over time.

These different pilot and commercial CO₂ storage projects allow us to better understand, interpret and compare some of our results.

The results presented for each study cited above can help in understanding a CO₂ leak through a carbonate shallow freshwater aquifer, however there are differences depending on the site studied. According to Keating et al. (2013), the real response of an aquifer will depend on both hydrological (flow in a heterogeneous medium) and geochemical processes (CO₂-water-rock interactions), variable in time and space. Changes in water formation are the main issue of storing CO₂ in shallow aquifers, as a small amount of CO₂ is enough to have a significant impact (Gaus, 2010). In addition, the intrusion of CO₂ will cause chemical imbalances and trigger various chemical reactions (Czernichowski-Lauriol et al., 2006). The spatial and temporal development of a gas plume will be a function of several spontaneous processes such as the solubility of CO₂, the leakage flux, the flow of groundwater (Carroll et al., 2009, 2014).

Thus, it is essential to monitor the geochemistry of shallow aquifers where CO₂ is sequestered and potentially leaked. According to Carroll et al. (2009), a successful surveillance program includes sampling before and after the injection. For this, one of the most widely used strategies is to analyze water quality (alkalinity, temperature, pH, etc.) and collect mineralogy data from aquifer sediments. As demonstrated in Lee et al (2016) work, these different monitoring tools make it possible to monitor the distribution, both spatial and temporal, of a CO₂ plume that leaks in a shallow freshwater aquifer. The use of noble gases can also be useful for monitoring a site as shown by the works of Cohen et al. (2013), Rillard et al. (2015) and Rhino et al. (2016). The latter monitored the spatiotemporal distribution of a gas plume while the CO₂ (g) was injected into the vadose zone. For example, following an injection test, Cohen et al. (2013) used noble gases (He, Ne) to define preferential path of CO₂ migration through the vadose zone. Ju et al. (2020) stress the importance of continuous monitoring in the vadose zone to characterize the “vertical” migration of degassed budget. A CO₂ leak and associated risks can be identified in relation to the baseline measurements. It is essential to determine how much CO₂ degassed

around a leak point and understand how the groundwater flow can influence its propagation (Ju et al., 2020).

This study (being part of the *Aquifer-CO₂ leak project*) aims to understand, quantify and model the environmental impact of an induced CO₂ leak on water quality in the carbonate freshwater aquifer and understand the CO₂-water-carbonate interactions on the pilot site of Saint-Emilion (Gironde, France).

The two particularities of this study are the carbonate composition (98 ± 2 % of calcite) and the shallow depth of the aquifer (the water table is about 21 m deep (Loisy et al., 2013)) where the CO₂ injection takes place, unlike the studies carried out on the Bozeman and Frio sites. There are few examples of CO₂ leakage into shallow aquifers but we did not find CO₂ leakage study made into carbonate aquifer. Ha et al. (2020) studied the spatiotemporal impact of a CO₂ leak on a shallow groundwater system. However, the main constituent materials of the aquifer are alumino-silicate minerals, and the characterization of the leak took place at the laboratory scale, thanks to column experiments (push-and-pull tests). Wang et al. (2016) are also interested in a limestone aquifer (unconfined oxidizing carbonate aquifer) and assesses the impact of a potential CO₂ leak (variation in pH, mobilization of major, minor and trace elements) *via* batch and column experiments. Mickler et al. (2014), were interested in the impact of CO₂ on the mineral's dissolution and the precipitation of authigenic mineral phases of a sample of siliciclastic core from a depth of 2 806 m by XRD and SEM analyzes. Yang et al. (2014b) and Zhu et al. (2015) both carried out field-scale CO₂ injection experiments. For the first authors, the aquifer is shallow and of the siliciclastic type (50 % quartz, 17 % calcite, and others minerals) with a pulselike CO₂-release. The latter injected 27 tonnes of gaseous CO₂ into an aquifer about 180 m below a surface. The injection layer being mainly made up of fine sand (quartz, feldspars, clay minerals, etc.).

In addition, the carbonate aquifer studied in this work is subject to its own hydrological characteristics and allows rapid hydrogeochemical reactions between CO₂, water and rock. Its high heterogeneous petrophysical properties over a short distance allow multiple propagation pathways for the CO₂ plume, with a high porosity values ranging between 20 % to 43 % and a high permeability values varying between 1 and 26 D.

During the injection experiment, the impact of CO₂ on the water geochemistry and physicochemical parameters of the aquifer was studied. Through the different wells, this characterization enabled us to follow both spatially and temporally the dissolved gas plume migration, and to quantify its extent across the hydrosystem.

A presentation of the carbonate hydrosystem is shown initially. The experiment set-up and a preliminary salt experiment (performed before CO₂ injection) are explained in a second step. The results obtained in the field, in the laboratory and by modeling are then presented, interpreted and discussed.

2. Underground natural site setting

2.1 Geographical, geological and hydrological context

The experimental site is located in the south-west of France, in the Nouvelle-Aquitaine region, in the village of Saint-Emilion, Gironde (**Fig. 1**). The experimental site is located in the abandoned limestone underground quarry, exploited according to the “rooms and pillars” method. It was previously exploited on two levels (to 8 m and 16 m deep on average) which serve as an underground laboratory (**Fig. 2.a**). Our experiments are at level 2 (**Fig. 2**). The limestones of the underground quarry (our zone about 20 m thickness) is dated from the Upper

1b Oligocene (Stampien; 28-30 Ma). The facies vary from wackestone to grainstone, and are associated with high values of porosity (ranging from 20 to 45%) and permeability (between 2 and 18 D; **Figs. 2.b and 2.d**). Petrophysical parameters where the experiment took place in the saturated zone are ranging from 20 to 43 % for the porosity and from 1 to 26 D for the permeability (**Fig. 2.d**). Oligocene limestones have their fractures filled by impermeable red clays. Thereby, the porosity is only represented by a matrix pore network (Cerepi et al., 1998), where the variation in space can be explained by its heterogeneity and/or the alteration of rock (Rillard et al., 2015). Calcimetry measurements show that the CaCO₃ content of the limestones is about 98 ± 2%.

This hydrogeological system (**Fig. 2**) is composed (from the surface to the aquifer) of i) 0.30 m of soils (Cambisol calcareic type; IUSS Working Group WRB, 2007), approximately ii) 18 m of unsaturated oligocene limestones, and iii) the saturated zone (with a thickness of approximately 3 m depending on the aquifer recharge). The entirety of this formation covers a layer of green sannoisian marls. The unsaturated zone is composed by the evapotranspiration zone and the transition zone (comprising the capillary fringe). We consider that it is the lower limit of the capillary fringe which marks the beginning of the saturated zone. The water saturation of the unsaturated zone seasonally ranges from 15 and 50% (Cohen et al., 2013; Loisy et al., 2013). The reference well (called P6 in the figure) crosses the unsaturated and saturated zones, and allows the collection of water samples directly from the aquifer. The water table flows from NW to SE (**Fig. 3.a**), with a hydraulic gradient ranging from 2% (lowest water table elevation) to 5% (highest water table elevation). The level of the water table oscillates between 61 and 62.4 m NGF.

At the time of the CO₂ injection experiment (July, 2019), the water table level was at its lowest, with a hydraulic gradient of 2% and a water table elevation of 61.4 m NGF.

2.2 Characteristics of the experiment and tools used

Field and laboratory measurements

To carry out the CO₂ injection experiment in the carbonate shallow freshwater aquifer, eight wells were drilled: an injection well (named F1) and seven observation wells (named from F2 to F8; **Fig. 3**). These drillings are between 5 and 6 m long, with an 8 cm diameter. According to the same figure, the wells are arranged according to the flow of the aquifer. Using a single plane for reference, the distances from F1 to each well are as follows: 0.93 m for F2-F1; 2.50 m for F3-F1; 3.57 m for F4-F1; 2.56 m for F5-F1; 3.86 m for F6-F1; 5.30 m for F7-F1 and 7.10 m for F8-F1 (**Tab. 1**). Wells F1, F2, F3, F6, F7 and F8 are arranged on the same axis and wells F4 and F5 are lateral. In addition, well F2 is slightly shifted to the NE (**Fig. 3**).

Wells F1-F2-F3-F6-F8 are equipped with two types of probes (**Fig. 3.c**): i) a multiparameter probe (Aqua Troll 600, In-Situ) that is immersed continuously in the aquifer, and carries out physicochemical intermittent measurements every 30 min (electrical conductivity ($\pm 0.5\%$ of reading plus $1.0 \mu\text{S}\cdot\text{cm}^{-1}$), pH (± 0.1 pH units) and oxidation-reduction potential (ORP, ± 5.0 mV); ii) a probe (InPro 5000i, Mettler Toledo), also immersed in the aquifer, measures dissolved CO₂ concentrations in water ($\pm 10\%$ (pCO₂ 10-900 mbar)) at an identical time rate. The measurement range of the CO₂ probe varies between 0 and 20%. Beyond 20%, the recorded values are “saturated” and indicate a ceiling value. Some wells are also equipped with 9 electrodes immersed at different depths in the water table, making it possible to carry out electrical resistivity tomography measurements (this will be the subject of another study). To allow the device to be sealed, a packer (or inflatable stoppers) is placed above the water table

in each well, forcing the injected dissolved gas plume to flow into the carbonate freshwater aquifer. This avoids any degassing to the atmosphere.

All wells are equipped with tubing, allowing water sampling for geochemical analyses. Samples are taken at two different depths, 25 cm (series samples E1) and 70 cm (series samples E2) below the level of the water table. Samples are taken with a syringe and filtered (Minisart, 0.2 μm). In the laboratory, they are analyzed by ion chromatography (DIONEX IC-25, DIONEX SA, France) in order to quantify the cations and the anions (mg.L^{-1} , $\pm 5\%$). Simultaneously, the water alkalinity is measured, using a pH-meter (Consort, $\pm 0.2\%$). The titration solution corresponds to 0.1 L hydrochloric acid.

To study the geochemistry of major elements, water samples were taken three times in 24 h, every day for three weeks. This makes it possible to observe significant variations in concentrations. For technical reasons (staff available for sampling, cost of equipment, laboratory analyzes, etc.) the frequency of sampling could not be higher.

The CO_2 injection started on July 9, 2019 at 10 am and finished at 11:30 am. This corresponds to the time t_0 of the experiment, which will be taken as a reference to describe the different results. The gas bottle of 50 L (including a mixture of 90% of CO_2 , 9% of He and 1% of Kr) was bubbled into a tank containing 200 L of aquifer water (the results of these rare gases will be the subject of another article comparing different tracers between them). A stirring blade inside the tank helped the dissolution of the gas in the water before the start of the injection. A valve allowed the flow regulation, and a manometer made it possible to control the flow continuously. The water/dissolved gas mixture was then injected over 1 h 30 min into well F1, using a flow of approximately 2.20 L/min. The physicochemical parameters of the tank are: i) before adding the gas mixture to the 200 L of water: $\text{pH} = 7.27$ and conductivity = $649 \mu\text{s.cm}^{-1}$; ii) 200 L of water with the dissolved gas: $\text{pH} = 5.45$ and conductivity = $645 \mu\text{s.cm}^{-1}$ (**Tab. 2**).

Hydrodynamic and geochemical characterization of the carbonate freshwater aquifer: tracing with salt

A preliminary experiment which took place on March 29, 2019 verified the connectivity between the wells of the carbonate freshwater aquifer. For this, 200 L of a concentrated solution of 2 g/L of NaCl was injected directly into the aquifer from F1 at 4.20 L/min, and the electrical conductivity was measured in the various boreholes over time. The measurements were carried out with a multiparameter probe (submerged in well F1) and CTD-divers ($\sim 1\text{-}100 \mu\text{S}\cdot\text{cm}^{-1}$), placed in the other wells.

First, we can note that the baseline value of electrical conductivity is variable in the aquifer. Thus, the initial electrical conductivity is $652 \mu\text{S}\cdot\text{cm}^{-1}$ for well F1, $591 \mu\text{S}\cdot\text{cm}^{-1}$ for well F2, and $656 \mu\text{S}\cdot\text{cm}^{-1}$ and $543 \mu\text{S}\cdot\text{cm}^{-1}$ for wells F3 and F4. The baseline value of electrical conductivity is significantly higher in well F8 and should be around $718 \mu\text{S}\cdot\text{cm}^{-1}$.

Well F1 recorded the maximum electrical conductivity ($4400 \mu\text{S}\cdot\text{cm}^{-1}$), only few minutes after injection (**Fig. 4 and Tab. 1**). Wells F2, F3, F4, F6, F7 and F8 recorded maximum electrical conductivity values of 735, 1119, 559, 764, 686 and $753 \mu\text{S}\cdot\text{cm}^{-1}$ respectively (**Fig. 4 and Tab. 1**). Well F2 registered a maximum conductivity lower than that measured in well F3. This may be related to the position of the well F2 on the axis F1-F8 which is slightly offset, and therefore does not lie in the main flow direction of the water table.

In the well F4, the electrical conductivity was practically not influenced by the NaCl injection: in fact, the further the wells are from the injection point, the weaker is the recorded signal (large

amplitude). Therefore, the CO₂ plume would not flow laterally due to sufficient hydraulic gradient.

According to **figure 4**, the shape of the electrical conductivity curve for wells F1, F2, F3 and F6 shows a shoulder, of a slight increase in the electrical conductivity values. This second growth is probably related to the complexity of the porous medium in terms of porosity (see section 3.1). This could explain variable water circulation velocity along the F1-F8 axis. Wells F7 and F8, located further from the injection site, have a much more spread signal and this shoulder is much less visible. This could be masked by the homogenization and dissipation of the signal in time and space. Therefore, the longitudinal CO₂ plume dispersion is significant between wells F1 to F6, i.e. up to a distance of 3.86 m.

The velocity flow of the water (**Tab. 1**) calculated between each well over the distance F1-F8 is not constant: the NaCl plume spread at 0.50 m/day to cover the distance F1-F2, 1.15 m/day for the distance F1-F3, 0.57 m/day and 0.96 m/day for the distance F1-F4 and F1-F6 respectively, and finally 0.56 m/day to realize the distance F1-F8.

Therefore, this preliminary experience characterizes the advection of our carbonate freshwater aquifer.

3. Results

3.1 Dynamics of gasified water plume from evolution of physicochemical parameters in carbonate freshwater aquifer

The evolution of the physicochemical parameters of the gasified water plume are monitored and described from July 8, 2019 for wells F1, F2, F3, F6 and F8. They are represented in **figure 5**. The physicochemical parameters recorded before injection (baseline) are shown in **table 2** for wells F1, F2, F3, F6 and F8. It is important to specify that the baseline carried out five days before the injection experiment is sufficient compared to the hydrological variability of the water table over one year and to twenty-one days of our CO₂ experiment. Indeed, if the annual baseline is chosen to compare the results, the values of the experiment can be confused with the annual baseline. Finally, the maximum value reached for each physicochemical parameter during the injection experiment is also reported in **table 2** for the same wells.

The physicochemical parameters of the baseline highlight a very small heterogeneity of the carbonate freshwater aquifer. Initially, according to **table 2**, the pH varies in the range between 7.02 for well F1 and 7.15 for well F3. Before injection, the initial CO₂ concentrations were relatively close, between 1.84% for well F2 and 2.46% for well F1. The ORP measurement was variable from one well to another, and ranged from 233 mV for well F6 to 376 mV for well F8. These two ORP values vary in opposite directions. This heterogeneity can be explained by different microbiological activities between the wells. Moreover, according to **table 2**, the well F1 is the one which recorded the highest baseline values in terms of electrical conductivity. The electrical conductivity was the parameter with the most disparity: between 632 $\mu\text{S}\cdot\text{cm}^{-1}$ for well F3 to 738 $\mu\text{S}\cdot\text{cm}^{-1}$ to well F1.

The **figure 5.a** shows the evolution of CO₂ concentrations in the carbonate freshwater aquifer over time for wells F1, F2, F3, F6 and F8. After the CO₂ injection, the CO₂ concentrations in well F1 increased sharply, until the probe was saturated at 20% of CO₂ (a plateau is reached). The CO₂ concentrations in well F1 undoubtedly reached greater than 19.7% but couldn't be

effectively measured: it should be recorded between 0.07 days and 0.55 days after t_0 . The CO₂ probe in well F2 recorded a maximum CO₂ concentration 3.54%, 1.36 days after F1. The CO₂ concentration in well F3, reached 3.67%, 2.75 days after F1 (**Tab. 1**). The well F8 gave a very weak response with a maximum concentration of CO₂ not detectable.

The other physicochemical parameters measured reacted synchronously to the increase of CO₂ concentrations in the carbonate freshwater aquifer. According to the **figure 5.b**, in well F1, the maximum electrical conductivity, of 1551 $\mu\text{S}\cdot\text{cm}^{-1}$, is recorded only 7 hours after t_0 . Respectively, in the well F3, F6 and F8 (**Tab. 1**), the maximum electrical conductivity was 729 $\mu\text{S}\cdot\text{cm}^{-1}$, 2.45 days after F1, 716 $\mu\text{S}\cdot\text{cm}^{-1}$, 5.46 days after F1, and 777 $\mu\text{S}\cdot\text{cm}^{-1}$, 13.50 days after well F1.

In the wells F1, F3, F6 and F8 (**Tab. 1**), the minimum pH values were recorded synchronously with the maximum values of electrical conductivity (**Fig. 5.c**). The probe of well F1 measured a minimum pH value 5.63 just 30 minutes after t_0 . In the F3 well, probe registered a minimum pH value 6.97, just 2.85 days after F1. F6 reported a maximum decrease 5.67 days after well F1 (pH = 6.96). Finally, the probe in well F8 recorded a minimum pH value 7.07, 14 days after well F1.

The **figure 5.d** shows the evolution of the ORP over time for the same wells. The minimal value of the ORP was recorded in the well F1 at 238 mV, 0.17 days after t_0 . The probes of the other wells did not record a significant variation in the ORP values.

During the CO₂ experiment, the heterogeneous nature of the carbonate system was further highlighted by the measurements in well F3, which presents a double pulse: two increases in electrical conductivity and two drops in pH values associated with two increases of CO₂ concentrations (**Fig. 5**). This could be explained by the heterogeneity in terms of permeability

of the carbonate system which is very important over a short distance: more than one water propagation path can be used to reach a well. In fact, the examples cited in the work of Smith et al. (2017) show that new pore spaces are created via preferential dissolution pathways after a CO₂ injection into a carbonate formation, leading to changes in permeability. In this same article, these authors discuss the evolution of carbonate permeability as a function of their physical and chemical heterogeneity (ie.: particle size distribution, pore connectivity, mineralogy, etc.). The works of Rhino (2017) has revealed two types of porosity (micro- and macro-porosity) using mercury porosimetry for Saint-Emilion limestone. The macro-porosity would feed the first arrival of water caused by the permeability, while the micro-porosity would cause a second arrival linked to the water trapped in the porous space. Cohen et al. (2013) also demonstrated the heterogeneity of the carbonate formation with preferential pathways for CO₂ and different tracer gases (Ar and He).

Compared to wells F1 and F3, well F6 shows a very slow rise in the recording of the maximum electrical conductivity and the minimum value of pH (about 3 days). This peak is spread over time and takes 6.06 days to return to its electrical conductivity baseline values and 3.48 days to return to pH baseline values.

Well F8 takes the longest to record a maximum value of electrical conductivity and to return to baseline values. This is also related to the fact that it is the well furthest from the injection point.

Thanks to the monitoring of the physicochemical parameters, the migration of the gasified water plume injected into well F1 could be followed-up, propagating first in well F2, then well F3 and well F6 and finally in well F8, following the hydraulic gradient of the carbonate freshwater aquifer. As the distance from well F1 increases, the greater the time lag to record these maximums increases. According to **table 1**, the velocity of the gasified water plume is

not constant over the F1-F8 axis. In fact, it takes 1.02 days to cover the distance F1-F3, 0.71 days for F1-F6 and 0.53 days for F1-F8.

In addition, proportionally the physicochemical parameters showed different ranges of attenuation in the recording signal depending on wells. The growth in CO₂ concentrations and electrical conductivity and the decline in pH values were less strong as the distance to the injection well increased. According to **figure 5**, the growth in CO₂ concentrations in well F1 was at least 88%, and was 48% for well F2 and 47% for well F3. Electrical conductivity increased by 52% in well F1, 13% in well F3, 7% in well F6 and 5% in well F8. Finally, pH values have decreased by 20% in well F1, 2% in well F3, 1% in well F6 and 0.4% in well F8. The strong variations of these different physicochemical parameters after CO₂ injection are significant: therefore, they can clearly be distinguished from the baseline values.

In conclusion, for all wells, the parameter that caused the largest increase in signal corresponds proportionally to the CO₂ concentrations followed by the electrical conductivity and the pH values. Thus, the in-situ measurement of CO₂ concentrations seems to be the most effective to detect a CO₂ leak.

Moreover, the time to return to baseline values increased as the distance from well F1 increased and is not synchronous for a same well according to the physicochemical parameter measured. For CO₂ concentrations, it took 2 and 6 days for wells F1 and F3 to return to baseline values. This cannot be calculated for the well F2 as there were no baseline concentrations.

For electrical conductivity, well F1 took 2 days to return to baseline values, 4 days for well F3 and 6 days for well F6. Finally, it took 3 days for wells F1 and F6 to return to pH baseline values and 4 days for well F3.

The time to return to baseline values is faster when a well is located near the injection point and for each physicochemical parameter, this return time to the baseline is correlated with the amplitude variation of the measured signal. For the well F1 for example, the parameter which returns most quickly to the baseline values corresponds to the CO₂ concentrations followed closely by the electrical conductivity and finally by the pH values.

To conclude, the injection of CO₂ into the carbonate freshwater aquifer strongly modifies the physicochemical parameters in particular through the CO₂ concentrations where the measured signal has the highest amplitude and attenuation. To a lesser extent, the electrical conductivity and the values of pH were also impacted. The disturbance is greatest near injection and the time for dissipation of the disturbance caused by the CO₂ intrusion is increasingly important as the distance from the injection well increases.

Thus, pH is an excellent direct indicator of gasified water plume into groundwater (Rillard et al., 2014) as well as the dissolved CO₂ concentrations (Yang et al., 2014a).

3.2 Impacts of the CO₂ leakage on geochemistry of the carbonate freshwater aquifer

The CO₂ injection in well F1 on July 9 caused a rapid change in the geochemistry of the carbonate freshwater aquifer. In three wells (F1, F2 and F3), a significant growth in cation and anion concentrations were recorded.

The different water geochemistry analysis show that the concentrations of cations and anions found in E1 are identical to those measured in E2. The **figure 6** points out an example of this calcium concentrations evolution for well F1. The small volume of the well should lead to a

very rapid chemical homogenization of the water. Thus, a possible geochemical stratification of the waters was not observed.

Figure 7 shows the evolution of the concentrations ($\text{mg/L} \pm 5\%$) of cations and anions over time, for the injection well F1 and the observation wells F2 and F3. The results start from July 8, 2019 and are presented for a period of 20 days. In the **table 3**, the baseline concentrations for the cations and anions and the time of the recording of the maximum concentrations are presented for wells F1, F2 and F3. The results are not presented for wells ranging from F4 to F8 as no variation in ionic concentrations was measured in the time. Therefore, given the parameters of our experience, the geochemical influence of our CO_2 injection is not observed beyond well F3 (2.5 m long) (see the graphs of well F8 on **figure 7**).

According to the **figure 7** and the **table 3**, once the injection was complete, the CO_2 reacted very quickly with the carbonate freshwater aquifer. All ionic species recorded maximum concentration values then return to their baseline value or reach a plateau which may be higher or lower than the baseline. The first maximum value of concentrations is recorded in the well F1. Wells F2 and F3 reacted similarly to the injection well but with a mitigated signal. According to the **table 3**, ionic concentrations in wells F2 and F3 increased in the same way, but less strongly than in well F1. Indeed, an attenuation of the maximum concentration peak is measured progressively as the distance from the injection point increases. In the same way, this peak is recorded in a time-shifted manner. In addition, in the well F3, the maximum ionic concentrations were more spread successively over time. Depending on the ionic species, certain maximums occurred before or after those of well F2.

For well F1, Ca^{2+} recorded maximum concentration values 0.33 days after t_0 , with a 47% increase in concentrations. After this maximal peak, Ca^{2+} return to its baseline value and remain constant. For this, it took 0.67 days. For wells F2, F3 and F8, 1.01, 3.02 and 13.53 days after t_0 , Ca^{2+} concentrations increased by 27%, 26% and 17% respectively.

HCO_3^- recorded maximum concentration values 0.33 days after t_0 in well F1, with an increase of 62%. After this first maximal peak, it took 1.33 days for HCO_3^- to recover a stabilization. 14.5 days after t_0 , the concentrations remain constant. For wells F2, F3 and F8, HCO_3^- recorded a maximum concentration 1.67, 2.02 and 13.53 days after CO_2 injection and increased by 23%, 18% and 6% respectively.

For well F1, Na^+ recorded maximum concentration values 0.33 days after t_0 with an increase in concentrations of 65%. After this maximal peak, it took 0.67 days for Na^+ to recover a stabilization. 14.5 days after t_0 , a new variation of concentrations is measured with a decrease from 11 mg/L to 9 mg/L (decrease of 22%). For well F2, 1.01 days after t_0 , Na^+ concentrations increased by 8%. For well F3, 0.69 days after t_0 , its concentrations increased by 8%: same increase as for well F2 but 0.32 days earlier. 14.5 days after t_0 , the concentrations decreased by 25% for well F2 and by 38% for well F3. In well F8, the Na^+ concentrations decrease by 3%, 12.49 days after injection.

For well F1, Mg^{2+} recorded maximum concentration values 0.33 days after t_0 and increase by 25%. It has proportionally to the other ionic species little increased. It took 0.34 days for Mg^{2+} to recover a stabilization. 14.5 days after t_0 its concentrations remain constant. For wells F2 and F3, 1.01 and 2.02 days after t_0 respectively, Mg^{2+} concentrations increased by 25%. Finally, 12.49 days after t_0 , the concentrations increased by 12% in well F8.

K^+ recorded maximum concentration values 0.33 days after t_0 in well F1 with an increase of 89%. K^+ has proportionally to the other ionic species little increased. Then, it took 3.02 days to recover a stabilization. 14.5 days after t_0 , K^+ decreased from 1.2 mg/L to 0.8 mg/L (decrease of 50%). K^+ recorded a maximum concentration 1.67 days after CO_2 injection and increased by 67% in well F2. 1.35 days after t_0 , its concentrations increased up to 68% in well F3: same increase but 0.32 days earlier than well F2. 12.49 days after t_0 , the concentrations of K^+ increased until 1.62 mg/L in well F8.

The maximum concentrations of SO_4^{2-} was recorded 3.35 days after t_0 in well F1, with an increase of 43%. Then, it took 3.35 days for SO_4^{2-} to reach a stabilization of concentrations. 14.5 days after t_0 , its concentrations decreased from 67 mg/L to 62 mg/L (decrease of 8%). For well F2, 3.01 after t_0 , SO_4^{2-} concentrations reached a level and increased by 30%. In well F3, its concentrations increased by 23% 6 days after t_0 . 14.5 days after t_0 , the SO_4^{2-} concentrations decreased by 10% and 3% for wells F2 and F3 respectively. In well F8, 12.49 days after t_0 , concentrations increased by 20%.

The maximum concentrations of NO_3^- was recorded 3.35 days after t_0 in well F1, with an increase of 31%. Then, it took 3.35 days for NO_3^- to reach a stabilization of concentrations. 14.5 days after t_0 , its concentrations increased from 28 mg/L to 41 mg/L (increase of 32%). In wells F2 and F3, 4.65 and 3.66 days after CO_2 injection, NO_3^- concentrations increased gradually by 39% and 29% respectively. 14.5 days after t_0 , its concentrations increased by 16% and 22% for wells F2 and F3. In well F8, 12.49 days after t_0 , the concentrations of NO_3^- increased by 40%.

Cl⁻ recorded maximum concentration values only 0.33 days after t₀ in well F1, with an increase of 39%. Then, it took 3.35 days for Cl⁻ to reach a stabilization of concentrations. 14.5 days after t₀, its concentrations increased from 19 mg/L to 33 mg/L (increase of 42%). For wells F2 and F3, 1.01 and 7.05 days after t₀, Cl⁻ concentrations increased by 24% and 14% respectively. 14.5 days after t₀, its concentrations increased by 21% for well F2 and by 36% and for well F3. In well F8, 12.49 days after t₀, the concentrations of Cl⁻ increased by 9%.

The reason for the increase in Cl⁻ concentrations is poorly understood. Other studies have also noted increases in Cl⁻ after CO₂ injection like Yang et al. (2013) and Zhu et al. (2015), but according to these latter; “the cause of these shifts of Cl concentration is unclear”. Gaus (2010) indicates that, in the case of a brine and freshwater aquifer, the chloride concentrations increase after alteration of clay minerals linked to the CO₂ injection. Kaszuba et al. (2003) indicate that the concentration of the brine itself at high pressures and temperatures causes the increase in Cl⁻ concentrations (see references therein).

To conclude, the further the distance to the injection point, the greater the respective arrival times of the maximum ion concentrations. Thus, for well F1, the maximum concentrations arrive over two periods and are recorded at 0.33 days (for Ca²⁺, HCO₃⁻, Na⁺, Mg²⁺, K⁺ and Cl⁻) and at 3.35 days (for SO₄²⁻ et NO₃⁻). For well F2, these arrive over four periods: at 1.01 days (for Ca²⁺, Na⁺, Mg²⁺ and Cl⁻), 1.67 days (for HCO₃⁻ and K⁺), 3.01 days (for SO₄²⁻) and at 4.65 days (for NO₃⁻). Finally, for well F3, the maximum concentrations arrive over seven periods: at 0.69 days (for Na⁺), 1.35 days (for K⁺), 2.02 days (for Mg²⁺ and HCO₃⁻), 3 days (for Ca²⁺), 3.66 days (for NO₃⁻), 6 days (for SO₄²⁻), and at 7.05 days (for Cl⁻).

The time to return to baseline or plateau values is variable depending on the well F2 and F3 (**Fig. 7 and Tab. 3**). After recording a maximum concentration value, it took 2.32 days for

HCO_3^- for well F2 against 5.03 days for well F3. Ca^{2+} concentrations took 2.35 days to return to plateau values over the baseline for the two wells, whereas Na^+ took 2.35 days for well F2 against 3.68 in well F3 to return to plateau values under the baseline. K^+ took 2.68 days to return to plateau values over the baseline for well F2 and 6.31 days for well F3. Finally, Mg^{2+} took 3.64 days for well F2 to return to baseline and 3.98 days for well F3. Note that for wells F1, F2 and F3 the order of return of the ions to baseline or plateau values is not identical. In addition, the baseline has not the value place for the same species on different wells (**Fig. 7 and Tab. 3**). According to Kharaka et al. (2010), variations in ionic concentrations can highlight local variations in the mineral composition of soils and sediments.

According to **figures 5 and 7**, the massive influx of CO_2 into well F1 lead to the rapid increase in concentrations of Ca^{2+} , HCO_3^- , K^+ , Na^+ , Mg^{2+} and Cl^- . This release in the aqueous phase caused a rapid decrease in pH values resulting to the acidification of the water. In addition, these concentrations have varied almost synchronously with increasing values of electrical conductivity and ORP. NO_3^- and SO_4^{2-} concentrations increased more gradually compared to others ions, offset from the CO_2 injection. Moreover, 14.5 days after t_0 , the low increase of NO_3^- and Cl^- concentrations was not recorded by the physicochemical parameters.

The maximum ionic concentrations recorded for well F2 and F3 are synchronous with the growth in CO_2 concentrations measured in both wells. As for the injection well and only measured for the well F3, the ions dissolution and the acidification of the water caused by the injection are accompanied by an increase in the electrical conductivity and a decrease in the pH values. The ORP measurement was not sensitive enough to detect these variations in concentration. The increase of Cl^- and NO_3^- , 14.5 days after the injection, was not recorded by the physicochemical parameters.

For well F8, as the increases in concentrations remain very small and close to the baseline values, these are not significant unlike wells F1, F2 and F3 (with the exception of concentrations of NO_3^- and SO_4^{2-}).

As the distance to the injection well increases, the time to record the peak concentration rises (delay) and there is an attenuation of the signal. Moreover, the time to return to the baseline also increases. This shows a certain inertia of the system (**Figs. 5 and 7**). However, this is not valid for Na^+ and SO_4^{2-} (and in a lesser degree K^+) whose concentrations increased even 14.5 days after injection, and for Cl^- and NO_3^- whose concentrations continued to grow.

In the conditions of our experiment, the increase in CO_2 concentrations in the injection well significantly modified the physicochemical parameters of the carbonate freshwater aquifer (**Fig. 5 and Tab. 2**), especially through the evolution of cation-anion concentrations. Thanks to the recording of the maximum concentration peak, the gasified water plume could be monitored in time and space, within a radius of influence of around 7.1 m. Indeed, the geochemical impact of the CO_2 intrusion was felt up to well F8, with an increasingly low concentration of cations and anions. To conclude, the propagation of the CO_2 plume takes place only longitudinally thanks to the hydraulic gradient of the water table. The monitoring of the different physicochemical parameters (**Fig. 5**) indicates that values increased and/or decreased over a period of two weeks. The concentration of major elements evolves in the same way (**Fig. 7**).

4. Interpretations and discussion

Comparison of salt tracing and CO_2 experiments

According to **figures 4 and 5**, in the NaCl and CO₂ injection experiments, the electrical conductivity curve have the same shape, with a shift and attenuation of the signal over time as the distance from the injection point increases. Between the wells, the curves show differences: a peak for F1, a peak followed of a shoulder for F3, a small shoulder followed of a sprawled peak for F6 and large and low peak for F8.

According to **figure 8**, for both experiences, the velocity decreased when the distance increased and gradually reflects the velocity of the water table at high scale (in well F8). Thus, NaCl and gasified water plumes propagated at a same range of velocity but with a faster velocity measured for the NaCl tracing. The slight differences in velocity between the two experiences could be related to the reaction of NaCl and CO₂ with the rock, modifying the permeability of the porous structure in both cases but in a different way (Peysson et al., 2011). The slowdown velocity for the gasified water plume is probably related to its reaction with water which would modify the thermodynamic equilibrium and cause dissolution of CO₂ as suggested by Cohen et al. (2013).

The transmissivities of the aquifer have been obtained from well pumping tests on different wells (wells F2 to F7). This resulted in calculation of permeabilities in the experimental area. These results are shown in **figure 8**. Permeability values are very high and varies between 26 D for well F6 to 41 D for well F7 with an average around of 33 D. Then, at this scale, the carbonate hydrosystem shows a certain physical heterogeneity. The flows through the carbonate freshwater aquifer doesn't only seem to be control by well permeabilities but sometimes by preferential circulations. Preferential propagation pathways linked to limestone anisotropy have also been demonstrated in the works of Cohen et al. (2013) and Rhino et al. (2016) in comparison to the preliminary numerical simulations performed by Garcia et al. (2013). Bevc

and Morrison (1991) carried out a salt injection experience in a freshwater aquifer. They highlighted the spread of the salt plume thanks to variations in electrical resistivity using a multi-channel borehole-to-surface system. The results have shown that it propagates according to high bulk transmissivity values and suggest strong channel flow paths.

In addition, have a look on the impact caused by the injection conditions. The injection creates a change in the instantaneous velocity field. Two phenomena occur during injection: a mass transfer which corresponds to the physical displacement of the injected fluid and a pressure transfer which causes a modification of the piezometric surface more or less marked according to the hydrodynamic properties of the water table.

In the case of the salt tracing experiment, the estimate of the disturbance associated with the mass transfer corresponds to a radius of 0.56 m with an actual circulation speed linked to injection into the well F1 of 1.94 m/days. The estimate of the overload at the injection well F1, associated with the pressure transfer corresponds to an increase in the dimension of the piezometric surface of 1.65 cm in well F1, 1.28 cm in well F6, 0.89 cm in well F7 and 0.56 cm in well F8. This is equivalent to an increase in the hydraulic gradient of 0.23%. In the case of the gasified water experiment, the estimate of the disturbance associated with the mass transfer corresponds to a radius of 0.51 m with a real speed of circulation linked to the injection into the well F1 of 0.88 m/days. The estimate of the overload at the injection well F1, associated with the pressure transfer corresponds to an increase in the dimension of the piezometric surface of 0.75 cm in well F1, 0.57 cm in well F6, 0.41 cm in well F7 and 0, 25 cm in well F8. This is equivalent to an increase in the hydraulic gradient of 0.11%. All these calculations therefore show that the injection conditions have a very small radius of action and impact which decreases very quickly after the end of the injection.

The transport of our plume in the aquifer from well F1 to well F8 is carried out by advection (mean hydraulic gradient of the water table) and by diffusion due to chemical modifications resulting from our injection. Therefore, with regard to the physical properties of the medium, the experimental injection conditions, the speed of the slower conductivity peak of the CO₂ experiment is simply explained by much greater conductivity gradients between the wells in the case of salt experience.

In the salt tracing experiment, the conductivity is related to the transport of the plume in the aquifer. In the gasified water experiment, the conductivity reflects the transport of the plume in the aquifer plus the reactive part of the plume with the carbonate reservoir.

Table 1 shows that along the F1-F8 axis, the conductivity rate calculated step by step between two wells does not keep the same changes in the two experiments. Between wells F1 and F3, the less significant variation in the conductivity rate in the case of the CO₂ experiment would be explained by the dissolution of the carbonates causing a brake on the decrease in the conductivity. Then beyond well F3, the conductivity rate is very low due to the return to conductivities very close to the baseline. Then, it becomes difficult to determine the share of transport and reaction. In the salt experiment, due to the higher initial conductivities, the conductivity rate becomes lower between wells F6 and F8 where we find the conductivities close to the baseline. Furthermore, the negative conductivity rate between wells F6 and F8 in the CO₂ experiment is linked to the natural conductivity of well F8 which is much higher than that measured in well F6.

Reverse modeling of gasified water plume from ionic concentrations and calculation of the calcite saturation index

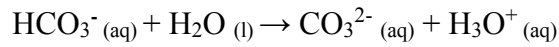
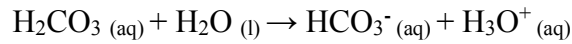
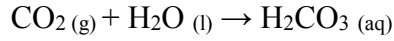
In this section, the experimental results from the CO₂ injection will be compared to calculated data with geochemical simulation software.

In our study, the water chemistry is mainly influenced by ion exchange and mineral dissolution mostly controlled by pH values. Initially, the water is in equilibrium with the reactive mineral phases present in the aquifer. The sharp increase in CO₂ concentration linked to its injection allows the CaCO₃-CO₂-H₂O reactions. This can be defined for wells F1, F2 and F3 thanks to pH and CO₂ concentrations measurements (**Fig. 5**). Beyond well F3, these reactions are difficult to determine because the measurements are within the detection limit of the multiparameter probe. Once injected in the well F1, the CO₂ (aq) is able to propagate in the aquifer thanks to the hydraulic gradient, locally modifying the physicochemical parameters measured in the others observation wells.

According to Dalton's law, the high CO₂ concentrations recorded after injection increase the CO₂ partial pressure (P_{CO2}) which will considerably and instantly modify the equilibria of the calco-carbonic system. The P_{CO2} is the main parameter controlling the groundwater pH, through the dissolution of gas phase CO₂. In addition, the depth location of an aquifer will also play a role on the P_{CO2}. In fact, this latter is higher for shallow aquifers, oscillating from 10⁻³ to 10⁻² atm (Appelo and Postma, 2005). During a leakage, it can vary between 10⁰ and 10^{2.5} atm, playing a major role on groundwater acidification (Cahill, 2013).

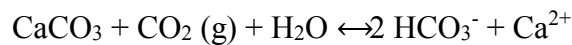
In our experience, during gasification of water before injection, the P_{CO2} is strong enough to cause a succession of chemical reactions in the carbonate system. In groundwater, the dissolution of CO₂ promotes a series of reactions:





Each time, the double dissociation of $\text{H}_2\text{CO}_3 (\text{aq})$ will release an H^+ ion (deprotonation reaction) further lowering the pH values of the solution. As the pH decreases, the concentrations of $\text{HCO}_3^- (\text{aq})$ decrease and those of $\text{CO}_2 (\text{aq})$ increase.

Moreover, if calcite is sufficiently present in the aquifer (even in excess), the CO_2 dissolution leads to calcite dissolution. After some time, although there is still dissolved CO_2 and solid CaCO_3 , a physicochemical equilibrium occurs:



Calcite dissolution can be highlighted by calculating the calcite saturation index (CSI) determined by PhreeqC. This index depends mainly on the ionic activity of the present chemical species (Plummer et al., 1978; Sigg et al., 2014) but also the temperature and pressure conditions of the medium. Thus, the saturation state of a solution is defined by:

$$\text{CSI} = \log \frac{Q}{K_s} = \log \frac{a_{\text{Ca}^{2+}} \times a_{\text{CO}_3^{2-}}}{K_s}$$

where CSI is the calcite saturation index, Q the ionic product of the solution, K_s the solubility coefficient of calcite and a_i the ionic activity coefficient of species i (Ca^{2+} and CO_3^{2-} in this case). If $\text{CSI} = 0$ (with $a_{\text{Ca}^{2+}} \times a_{\text{CO}_3^{2-}} = K_s$), the solute is in equilibrium with calcite. If $\text{CSI} < 0$, the solution is undersaturated and the calcite dissolves. If $\text{CSI} > 0$, the solution is supersaturated and calcite precipitates.

With PhreeqC, it is possible to recalculate the CO₂ concentrations (%) from the CO₂ saturation index (g) (for the pure phase in the aqueous phase) which corresponds to the decimal logarithm of the partial pressure of the gas component expressed in atmosphere (Thiéry, 2015). This calculated concentration will be directly compared to experimental results.

To calculate these two indexes, the PhreeqC inputs correspond to the experimental concentrations of anions and cations (F⁻, Cl⁻, NO₃⁻, SO₄²⁻, HCO₃⁻, Na⁺, K⁺, Mg²⁺, Ca²⁺; in mg/L) measured in each well associated with temperature and pH values (measured by the multiparameter probe).

Figure 9 presents the results of the CO₂ concentrations over time measured in the aquifer and recalculated by PhreeqC (from the CO₂ saturation index (g)), as well as the evolution of the CSI for wells F1, F2, F3 and F8. The curves correspond to the measurements made by the probe in each well, and the crosses correspond to the values calculated by PhreeqC.

First, the saturation index values calculated (**Fig. 9**) are not really significant to assert that the dissolution or precipitation of calcite are massive phenomena in the experiment because the values don't overstep 0.5 or -0.5. The CSI variations can only show an evolution tendency to dissolution or precipitation of calcite.

For the well F1, the measured and calculated CO₂ concentrations coincide perfectly: thus, the measurements performed by the probe may be utilized with confidence. As discussed in section 3.1, the growth in CO₂ concentrations in the carbonate freshwater aquifer during the injection was so high that the probe was saturated, failing to record the real maximum CO₂ concentrations values in well F1. The concordance of measured and calculated points shows a maximum concentration of almost 30% in CO₂ in the injection well. Following this, the CSI rapidly

decreased to -0.18, 0.67 days after CO₂ injection, showing a tendency to calcite dissolution. From 0.67 days to 3.65 days, the CSI values gradually rise, until equilibrium values are reached (CSI = 0.02). Then, the values remain in equilibrium and increase very slightly until 0.06. The sharp increase in CO₂ concentrations (up to 30%) at 0.33 days after injection is synchronous with the fall in CSI values (around -0.2). Similarly, the values of the CO₂ concentrations gradually return to equilibrium values as do the CSI values too.

In well F2, the CO₂ peak concentration calculated (2.93%) is lower than that measured (3.70%). Furthermore, the calculated CO₂ concentrations show a very unsettled evolution. The increase in CO₂ concentrations (from 2.27% to 4.16%) is accompanied by a drop in CSI values (from 0.06 to -0.06) from 0.68 days to 1.67 days after injection. Between 3.01 and 3.36 days, a drop in CO₂ concentrations is measured, with concentrations equal to 0.63%. In parallel, the CSI values increase to 0.63. From 3.35 days, the CO₂ concentrations increase in a chaotic trend and return to pre-injection values of around 2.5%.

In well F3, the CO₂ peak concentration calculated (4.20%) is higher than that measured (3.60%).

At 3.02 days, the increase in CO₂ concentrations calculated after injection (from 1.80% to 2.93%) causes a slight decrease in CSI values (from 0.10 to 0.08). The results showing a shoulder in values of electrical conductivity with a second increase (described in part 2.2) is also present for the CO₂ concentration values calculated by PhreeqC (which increase up to 2.33% between 5.03 and 5.36 days), accompanied by a very small decrease in CSI values (which decrease to 0.05). After 5.36 days, the CO₂ concentrations return to equilibrium values (to 1.7%) like the CSI values which are equal to 0.1.

The shoulder of the values described above could be linked to the water saturation in the limestone. The pores of the limestone rock can be blocked by this saturation preventing the diffusion of the gas for a certain time then release it later in a ventilation process (Cuezva et al., 2011). Depending on the solubility coefficients and diffusion phenomena in water, the gas transfer would be modified (Cohen et al., 2013).

Well F8 has a CO₂ concentration of around 2.5% and does not record a concentration peak. The associated CSI is equal to 0.

Modification of physicochemical parameters by spread of gasified water plume: reactions and/or transport process

These last results show that the main dissolution phenomenon takes place at the injection point consuming a large part of the dissolved CO₂: the CO₂ concentrations drop from 30% to 4% in 2.5 m.

In well F1, the lowest pH measured of a value of 5.63 led to the almost instantaneous dissolution of the limestones releasing Ca²⁺ and raised the pH. This leads to under saturation conditions only valid for pH below 6.3 in accord with the equilibrium in the calcocarbonic system. A similar case has been observed in the work of Zheng et al. (2012), where high levels of dissolved CO₂ did not cause a large decrease in pH values due to the buffering capacity of the aquifer and to the dissolution of calcite. The higher the sediment/water ratio is, the more the buffer capacity increases (Cahill, 2013). In our study, the buffering capacity of the carbonate hydrosystem is very fast because the CaCO₃ content of the limestones is about 98 ± 2%. This buffering capacity of the carbonate formation has also been demonstrated by Cohen et al. (2013). Following the injection of tracer gas (Ar, Ne, He) and CO₂ into limestone cavity, these authors have shown

that the tracers can propagate in the vadose zone and reach the surface which is not the case with CO₂ due to its dissolution and reaction with carbonate.

According to Thordsen (2011), the transport of dissolved CO₂ and the rapid flow of groundwater will cause high CO₂ concentrations and changes in water quality as for the works of Kharaka et al. (2010) for example. These authors also studied changes in groundwater quality following the controlled release of CO₂ by analyzing water samples taken before, during and after injection. In 2014, Carroll et al. showed that variations in pH values are strongly influenced by the lithology of the aquifer studied and depend on the transport of CO₂ by chemical solubility through it. In the case of deep CO₂ storage reservoir, these same authors have noticed that the contact between the rock of the aquifer and the wet supercritical CO₂ causes an increase in cation concentrations during batch experiments (Carroll et al., 2009). Other laboratory experiments have also observed these same phenomena (McGrath et al., 2007; Smyth et al., 2009, Lu et al., 2010, Little and Jackson, 2010). In our case, the release of ions in solution and the variations of the physicochemical parameters seen previously highlight the change in the type of water facies for wells F1, F2 and F3 (**Fig. 10**). Wells F1 and F3 have the same water evolution with a lower range for F3. Before injection and according to the baseline concentrations of cations and anions, the water is of the bi-carbonate calcium and magnesium type with HCO₃⁻ the dominant anion. Gradually, after CO₂ injection in the carbonate freshwater aquifer, the water facies moves toward the bi-carbonated calcium pole with a maximum at the peak of concentration. Afterwards, the facies gradually migrate in the opposite direction to the chlorinated-sulphated calcium pole. There is no return to the initial geochemical signature. The final facies is more chlorinated-sulphated calcium than the baseline facies. For well F2, the evolution of the facies is slightly different due to the continuation of the displacement of the

facies towards the bicarbonated calcium pole. It is only after that the facies moves towards the chlorinated-sulphated calcium pole and exceeds the facies of the baseline.

For the other CO₂ injection experiment from Kharaka et al. (2010) and Zheng et al. (2012), rapid and systematic changes in various physicochemical parameters (pH, alkalinity, electrical conductivity, etc.) were also reported after injection.

How can we explain that we do not get back the facies of the baseline and concentrations after the peak higher than the baseline as for SO₄²⁻, NO₃⁻, Ca²⁺, Cl⁻ and K⁺ or lower for Na⁺ (**Figs. 7 and 10**)?

In well F2, the higher concentrations of HCO₃⁻ based on the calculation thanks to the measurement of alkalinity are undoubtedly due to the proximity between wells F1 and F2 and a slight influence of the dissolved CO₂ would still be present. In well F3 more distant from well F1, this influence would no longer take place.

In wells F2, F3 and F6, the ion concentration peaks would correspond to the phenomenon of advection (**Fig. 7**). The non-return to the baseline concentration values would be explained by the slowness of the diffusion phenomena of part of the blocked fluid in a very complex porous medium. The return to equilibrium state depends on the chemical species and on several factors such as the distance from the injection point, the progressively diminution of CO₂ (aq) solubility, the pH buffering, and the groundwater flow which allows to progressively return to baseline values (Smyth et al., 2009). A longer geochemical monitoring through the various wells would allow to see if the initial concentrations can be getting back or if the stabilized values of the concentrations suggests that their mobilization is finished and the system has reached an approximate new equilibrium (Lu et al., 2010).

Furthermore at 14.5 days after CO₂ injection, the concentrations of NO₃⁻ and Cl⁻ brusquely increase and the concentrations of SO₄²⁻ and K⁺ decrease. A variation in the redox potential

could lead of this evolution (Rillard et al., 2014). Perhaps further geochemical modeling in transport-reaction could answer all these questions, as its been done in the work of Wang and Jaffe (2004), Carroll et al. (2009), Apps et al. (2010) and Wilkin and Digiulio (2010). Indeed, as the work of Carroll et al. (2014) suggests, groundwater chemistry can be impacted over several years, even if small amounts of CO₂ are injected.

Finally, electrical conductivity measurements are a useful tool to detect a CO₂ leak thanks to its synchronous variations with ionic and CO₂ concentrations as well as pH values. Indeed, it show a similar trend of bicarbonate ions and is very well correlated with calcium concentrations and perfectly anti-correlated with pH measurements (**Fig. 5**). In our case, electrical conductivity increased due to a growth in total dissolved solids (Cahill, 2013) linked to the dissolution of limestone, increasing ionic concentration of the aqueous solution (especially Ca²⁺ and HCO₃⁻). Any variations of electrical conductivity indicate changes in geophysical properties and chemical composition. This physicochemical parameter seems to be sensitive to the intrusion of CO₂ into a carbonate freshwater aquifer, making it a good marker in a leakage context.

5. Conclusion

A CO₂ leakage experiment in a shallow freshwater carbonate aquifer was carried out on July 9, 2019 in order to assess the potential impact of CO₂ on the groundwater chemistry. These results highlight different physicochemical tools that allow the detection and the monitoring of a gasified water plume through the hydrosystem, thanks to eight wells (one for injection, seven for observation).

We can conclude that, in our experimental conditions, five physicochemical parameters made it possible to predict and monitor the spread of a gasified water plume through a carbonate freshwater aquifer. Thus, the CO_2 (aq), the Ca^{2+} and HCO_3^- concentrations, the pH, and the electrical conductivity are considered as good markers, sufficiently sensitive and reactive, which can be used on CO_2 storage site in order to follow any physicochemical disturbance of a shallow carbonate freshwater aquifer.

Certainly, these physicochemical parameters are dependent on each other. However, the interest of this study is to show that geochemical tools (such as the probes used) allow continuous acquisition while being immersed in the aquifer, and make it possible to record the smallest variations of these parameters over time (ie: allows to see the heterogeneities of the carbonate hydrosystem for example, via two bumps of electrical conductivity measured in well F3).

Thus, according to this work, the parameters which are the most sensitive (in order of sensitivity) are: i) electrical conductivity: which is an indirect and independent measurement probe, which is not deducted from the material balance; ii) pH: measurement from pH probe independent measurement of the electrical conductivity probe; iii) CO_2 concentrations: measured from direct measurement probe but less sensitive than the previous two; iv) chemical concentrations such as those of Ca^{2+} (indirect measurement by laboratory analysis). These different parameters act here as a measurement and monitoring tool which react to a CO_2 leak.

The buffering capacity of a carbonate hydrosystem plays a key role in mitigating a CO_2 leak. A high buffering capacity will make it possible to reduce excessive acidification: the amount of reactive buffer carbonate minerals present is therefore an essential parameter to prevent a CO_2 leakage.

The reaction rates of these five physicochemical parameters cited above vary over time as a function of the distance between the monitoring wells and the injection point. The closer a monitoring well is to the injection well, the faster the physicochemical parameters will react to the intrusion of CO₂. This highlights the hydraulic gradient of the water table, which allows the gas plume to diffuse and flow through the hydrosystem. Sometimes, the heterogeneity of the carbonate massif in terms of petrophysical properties allows the gas to migrate through several different propagation paths, more or less quickly over a short distance.

The diminution of pH values caused by the increase in CO₂ concentrations (aq) lead to calcite dissolution, and generate calcium ions in solution, modifying the aqueous chemical response (Wang and Jaffe, 2004 and Cahill, 2013). Therefore, CO₂ (aq) will have a strong influence on the carbonate system and on water-rock interactions in shallow and potable aquifer systems (Cahill, 2013). This phenomenon takes the form of a decrease in pH values (up to 5.63) and an increase in bicarbonate ions (up to 350 mg/L), by increasing the partial pressure of CO₂. In addition, these chemical processes require significant ion exchanges recorded by electrical conductivity which systematically increases when a maximum of CO₂ (aq) is recorded.

However, the calcite saturation index shows that the system is in equilibrium (except for the injection well F1). This implies that the calcite dissolution caused by the reaction of CO₂-CaCO₃-H₂O system takes place only in well F1: chemical reactions have a relatively rapid kinetics. The variations of the different physicochemical parameters in the others wells are only related to the transport of CO₂ (aq) by advection and diffusion thanks to the groundwater flow.

This also highlights the strong buffering capacity of the carbonate hydrosystem which makes it possible to minimize the propagation of CO₂. For this experiment, these reaction processes occurred mainly after the injection. In this well buffered carbonate hydrosystem, the gas plume

may reach very high levels in some places, due to geological heterogeneity, hydrodynamic factors and/or spatial variations in the flow of CO₂ (Keating et al., 2010). High buffering aquifers are therefore the most effective systems for mitigating the negative effects of CO₂ intrusions (Wang and Jaffe, 2004).

In term of recommendations, in order to acquire the maximum information related to the spatial propagation of a gas plume, it is necessary to install several observation wells located near the injection point, especially if the volume of gas injected is not very high. Indeed, the physicochemical reactions occur very quickly after the CO₂ injection and the signals are rapidly attenuated due to the buffering capacity of the carbonate hydrosystem. Also, it is essential to use uninterrupted automated monitoring tools with the aim of recording each variation of the different physicochemical parameters. Indeed, unexpected values can be measured due to the petrophysical properties of the rock for example. Measurements that require laboratory treatment such as analyzes of major elements must be carried out as quickly as possible in order to avoid (i) possible degassing and (ii) the contact between the water sample and the atmosphere.

Addressing the challenges that storage sites face is complex. Considering the results presented in this study and the previous recommendations, there is a real challenge on a commercial scale for CCS sites. Monitoring shallow groundwater may not be the best approach to detect possible CO₂ leak from CCS reservoirs.

To maximize the chances of detecting a leak, it is essential to carry out interdisciplinary research, both fundamental and applied, covering the whole range of relevant scales (Jun et al., 2013). Field observations, laboratory demonstrations, and modeling would assess potential CO₂

leakage rates from a site, in order to obtain a permit where CO₂ injection should take place in reservoirs covered by potable aquifers (Gaus, 2010).

Aknowlegements

This research was conducted within the Aquifer-CO₂ Leak project and we thank the entire Aquifer-CO₂ Leak project team. This project is funded by ADEME and more particularly Aïcha El Khamlichi and the Nouvelle-Aquitaine Region, France. The authors are grateful to the IFP-EN and research unit EA 4592 “Géoressources et Environnement” – ENSEGID, Bordeaux INP for creating a supportive and exciting research environment.

Bibliography

1. Albritton, D.L., Meira Filho, L.G. (2001). Climate Change 2001: The Scientific Basis; Contribution of Working Group I to the Third Assessment Report of the Intergovernmental Panel on Climate Change - Technical Summary. Geneva: IPCC.
2. Ambats, G., Apps, J.A., Beers, S., Birkholzer, J.T., Gullickson, K.S., Herkelrath, W.N., Kakouros, E., Kharaka, Y.K., Spangler, Y.K., Spycher, L.H., Thordsen, J., Zheng, L. (2009). Groundwater chemistry changes as a result of CO₂ injection at the ZERT field site in Bozeman, Montana. Lawrence Berkeley National Laboratory. Project Report LBN, L-2931.
3. Appelo, C., Postma, D. (2005). Geochemistry, Groundwater and Pollution, Second Edition (Taylor & Francis).
4. Apps, J.A., Zheng, L., Spycher, N., Birkholzer, J.T., Kharaka, Y., Thordsen, J., Kakouros, E., Trautz, R. (2011). Transient changes in shallow groundwater chemistry during the MSU ZERT CO₂ injection experiment. Energy Procedia 4, 3231–3238.
5. Bachu, S. (2008). CO₂ storage in geological media: Role, means, status and barriers to deployment. Progress in Energy and Combustion Sciences 34, 254-273.
6. Bevc, D., Morrison, H.F. (1991). Borehole-to-surface electrical resistivity monitoring of a salt water injection experiment. Geophysics, vol. 56, No. 6, 769-777.
7. Cahill, A.G. (2013). Hydrogeochemical impact of CO₂ leakage from geological sequestration on shallow potable aquifers. Kgs. Lyngby: DTU Environment.
8. Carroll, S.A. (2009). Trace metal release from Frio Sandstone reacted with CO₂ and 1.5N NaCl brine at 60°C. Eighth Annual Carbon Capture & Sequestration Conference, May 4-7, Pittsburgh, PA.

9. Carroll, S.A., Keating, E., Mansoor, K., Dai, Z., Sun, Y., Trainor-Guitton, W., Brown, C., Bacon, D. (2014). Key factors for determining groundwater impacts due to leakage from geologic carbon sequestration reservoirs. *International Journal of Greenhouse Gas Control* 29, 153-168.
10. Cerepi, A., Humbert, L., Burlot, R., Pouchan, P. (1998). Détermination de la teneur en eau d'un milieu poreux non saturé en utilisant Time Domain Reflectometry. *Bulletin of Engineering Geology and the Environment* 57, 69–78.
11. Cohen, G. Loisy, C., Laveuf, C., Le Roux, O., Delaplace, P., Magnier, C., Rouchon, V., Garcia, B., Cerepi, A. (2013). The CO₂-Vadose project: Experimental study and modelling of CO₂ induced leakage and tracers associated in the carbonate vadose zone. *International Journal of Greenhouse Gas Control* 14, 128-140.
12. Cuezva, S., Fernandez-Cortes, A., Benavente, D., Serrano-Ortiz, P., Kowalski, A., Sanchez-Moral, S. (2011). Short-term CO₂ (g) exchange between a shallow karstic cavity and the external atmosphere during summer: role of the subsurface soil layer. *Atmospheric Environment* 45, 1418-1427.
13. Czernichowski-Lauriol, I., Rochelle, C., Gaus, I., Azaroual, M., Pearce, J., Durst, P. (2006). Geochemical interactions between CO₂, pore-waters and reservoir rocks. In: *Advances in the geological storage of carbon dioxide*. Springer, Dordrecht, 157-174.
14. Gale, J. (2004). Geological storage of CO₂: what do we know, where are the gaps and what more needs to be done? *Energy* 9-10 29, 1330-1338.
15. Gaus, I. (2010). Role and impact of CO₂-rock interactions during CO₂ storage in sedimentary rocks. *International Journal of Greenhouse Gas Control* 4, 73-89.
16. Ha, J. H., Jeon, S. W., Hwang, H. T., Lee, K. K. (2020). Changes in geochemical and carbon isotopic compositions during reactions of CO₂-saturated groundwater with aquifer materials. *International Journal of Greenhouse Gas Control* 95, 102961.

17. Hepple, R.P., Benson, S.M. (2005). Geologic storage of carbon dioxide as a climate change mitigation strategy: performance requirements and the implications of surface seepage. *Environmental Geology*, 576-585.
18. Holloway, S. (1997a). An overview of the underground disposal of carbon dioxide. *Energy Conversion and Management* 38 (SS), S193-S198.
19. Holloway, S. (1997b). Safety of the underground disposal of carbon dioxide. *Energy Conversion and Management* 38 (SS), S241-S245.
20. Holloway, S., Pearce, J.M., Hards, V.L., Ohsumi, T., Gale, J. (2007). Natural emissions of CO₂ from the geosphere and their bearing on the geological storage of carbon dioxide. *Energy* 32, 1194-1201.
21. Hovorka, S.D., Benson, S.M., Doughty, C., Freifeld, B.M., Sakurai, S., Daley, T.M., Kharaka, Y.K., Holtz, M.H., Trautz, R.C., Seay Nance, H., Myer, L.R., Knauss, K.G. (2006). Measuring permanence of CO₂ storage in saline formations: the Frio experiment. *Environmental Geosciences* 13 (2), 105-121.
22. IPCC (1997). Stabilisation des gaz atmosphériques à effet de serre : conséquences physiques, biologiques et socio-économiques. Document technique III du GIEC.
23. IPCC (2005). Carbon Dioxide Capture and Storage. Cambridge University Press, New York, U.S.A.
24. IPCC (2014). Climate Change 2014: Synthesis Report. Contribution of Working Groups I, II and III to the Fifth Assessment Report of the Intergovernmental Panel on Climate Change IPCC, Geneva, Switzerland, 151.
25. Ju, Y., Gilfillan, S., Lee, S.S., Kaown, D., Hahm, D., Lee, S., Park, I.W., Ha, S.W., Park, K., Do, H.K., Yun, S.T., Lee, K.K. (2020). Application of noble gas tracers to identify the retention mechanisms of CO₂ migrated from a deep reservoir into shallow groundwater. *International Journal of Greenhouse Gas Control*, vol. 97, 103041.

26. Jun, Y.S., Giammar, D.E., Werth, C.J. (2013). Impacts of geochemical reactions on geologic carbon sequestration.
27. Kaszuba, J. P., Janecky, D. R., Snow, M. G. (2003). Carbon dioxide reaction processes in a model brine aquifer at 200°C and 200 bars: implications for geologic sequestration of carbon. *Applied Geochemistry* 18(7), 1065-1080.
28. Kharaka, Y.K., Cole, D.R., Hovorka, S.D., Gunter, W.D., Knauss, K.G., Freifeld, B.M. (2006). Gas-water-rock interactions in Frio Formation following CO₂ injection: implications for the storage of greenhouse gases in sedimentary basins. *Geology* 34, 577-580.
29. Kharaka, Y.K., Yousif, K., Thordsen, J.J., Kakouros, E., Ambats, G., Herkelrath, W.N., Beers, S.R., Birkholzer, J.T., Apps, J.A., Spycher, N.F., Zheng, L., Trautz, R.C., Rauch, H.W., Gullickson, K.S. (2010). Changes in the chemistry of shallow groundwater related to the 2008 injection of CO₂ at the ZERT field site, Bozeman, Montana. *Environmental Earth Sciences*, vol. 60, No. 2, 273-284.
30. Keating, E.H., Fessenden, J., Kanjorski, N., Koning, D.J., Pawar, R. (2010). The Impact of CO₂ on Shallow Groundwater Chemistry: Observations at a Natural Analog Site and Implications for Carbon Sequestration. *Environmental Earth Sciences* 60:521-536.
31. Keating, E.H., Hakala, J.A., Viswanathan, H., Carey, J.W., Pawar, R., Guthrie, G.D., Fessenden-Rahn, J. (2013). CO₂ leakage impacts on shallow groundwater: Field-scale reactive-transport simulations informed by observations at a natural analog site. *Applied geochemistry*, 2013, vol. 30, 136-147.
32. Lee, K.K., Lee, S.H., Yun, S.T., Jeon, S.W. (2016). Shallow groundwater system monitoring on controlled CO₂ release sites: a review on field experimental methods and efforts for CO₂ leakage detection. *Geosciences Journal* vol. 20 (4), 569-583.

33. Lewicki, J.L., Birkholzer, J.T., Tsang, C.F. (2007). Natural and industrial analogues for leakage of CO₂ from storage reservoirs: identification of features, events, and processes and lessons learned. *Environmental Geology*, 52:457-467.
34. Lindeberg, E., Bergmo, P. (2003). The long-term fate of CO₂ injected into an aquifer. In: Gale, K., Kaya, Y., editors. *Greenhouse Gas Control Technologies*, vol. 1, 489-494.
35. Little, M.G., Jackson, R.B. (2010). Potential impacts of leakage from deep CO₂ geosequestration on overlying freshwater aquifers. *Environmental Science and Technology* 44 (23), 9225-9232.
36. Loisy, C., Cohen, G., Laveuf, C., Le Roux, O., Delaplace, P., Magnier, C., Rouchon, V., Cerepi, A., et Garcia, B. (2013). The CO₂-Vadose Project: Dynamics of the natural CO₂ in a carbonate vadose zone. *International Journal of Greenhouse Gas Control* 14, 97-112.
37. Lu, J.M., Partin, J.W., Hovorka, S.D., Wong, C. (2010). Potential risks to freshwater resources as a result of leakage from CO₂ geological storage: a batch-reaction experiment. *Environmental Earth Sciences* 60:335-348.
38. McGrath, A.E., Upson, G.L., Caldwell, M.D. (2007). Evaluation and mitigation of landfill gas impacts on cadmium leaching from native soils. *Ground Water Monitoring Remediation* 27, 99-109.
39. Mickler, P. J., Yang, C., Lu, J., Lankford, K. D. (2014). Laboratory batch experiments and geochemical modelling of water-rock-super critical CO₂ reactions in Gulf of Mexico Miocene rocks: implications for future CCS projects. *Energy procedia* 63, 5512-5521.
40. Myers, M., Roberts, J.J., White, C., Stalker, L. (2019). The impact of water on CO₂ leak rate measurements for CCS projects. In: 14th International Conference on Greenhouse Gas Control Technologies, Melbourne, Australia, 21-26 October 2018.

41. Oldenburg, C., Lewicki, J., Dobeck, L., Spangler, L. (2010). Modeling gas transport in the shallow subsurface during the ZERT CO₂ release test. *Transport Porous Media* 82 (1), 77-92.
42. Plummer, L.N., Wigley, T.M., Parkhurst, D.L. (1978). Critical review of the kinetics of calcite dissolution and precipitation.
43. Rhino, K., Loisy, C., Cerepi, A., Le Roux, O., Garcia, B., Rouchon, V., Noirez, S., Le Gallo, C., Delaplace, P., Willequet, O., Bertrand, C., El Khamlichi, A. (2016). The Demo-CO₂ project: Monitoring and comparison of two shallow subsurface CO₂ leakage experiments with gas tracer associated in the carbonate vadose zone. *International Journal of Greenhouse Gas Control*, vol. 53, 207-221.
44. Rhino, K. (2017). Caractérisation, quantification et modélisation des processus de transfert et des interactions CO₂-eau-roche en milieu poreux non saturé en contexte de forage lors d'un stockage géologique. Thèse de l'université de Bordeaux 3 - Michel de Montaigne.
45. Rillard, J., Gombert, P., Toulhoat, P., Zuddas, P. (2014). Geochemical assessment of CO₂ perturbation in a shallow aquifer evaluated by a push-pull field experiment. *International Journal of Greenhouse Gas Control*, vol. 21, 23-32.
46. Rillard, J., Loisy, C., Le Roux, O., Cerepi, A., Garcia, B., Noirez, S., Rouchon, V., Delaplace, P., Willequet, O., Bertrand, C. (2015). The Demo-CO₂ Project: A unsaturated zone CO₂ and tracer leakage field experiment. *International Journal of Greenhouse Gas Control* 39, 302-317.
47. Roberts, J.J., Stalker, L., Shipton, Z.K., Burnside, N.M. (2019). What have we learnt about CO₂ leakage in the context of commercial-scale CCS? In: 14th International Conference on Greenhouse Gas Control Technologies, Melbourne, Australia, 21-26 October 2018.

48. Sigg, L., Behra, P., Stumm, W., Amatore, C. (2014). Chimie des milieux aquatiques.
49. Smith, M.M., Hao, Y., Carroll, S.A. (2017). Development and calibration of a reactive transport model for carbonate reservoir porosity and permeability changes based on CO₂ core-flood experiments. *International Journal of Greenhouse Gas Control* 57, 73-88.
50. Smyth, R.C., Hovorka, W.D., Lu, J., Romanak, K.D., Partin, J.W.C., Yang, W.C. (2009). Assessing risk to fresh water resources from long term CO₂ injection-laboratory and field studies. *Energy Procedia* 1:1957-1964.
51. Strazisar, B.R., Wells, A.W., Diehl, J.R., Hammack, R.W., Veloski, G.A. (2009). Near-surface monitoring for the ZERT shallow CO₂ injection project. *International Journal of Greenhouse Gas Control* 3 (6), 736-744.
52. Thiéry, D. (2015). Modélisation 3D du Transport Réactif avec le code de calcul MARTHE v7.5 couplé aux modules géochimiques de PHREEQC. Rapport BRGM/RP-65010-FR, 167-188.
53. Thordsen, J. (2011). Personal communication in Zheng et al. (2012).
54. Wang, S., Jaffe, P.R. (2004). Dissolution of a mineral phase in potable aquifers due to CO₂ releases from deep formations: effect of dissolution kinetics. *Energy Conversion and Management* 45 (18-19), 2833-2848.
55. Wang, G., Qafoku, N. P., Lawter, A. R., Bowden, M., Harvey, O., Sullivan, C., Brown, C. F. (2016). Geochemical impacts of leaking CO₂ from subsurface storage reservoirs to an unconfined oxidizing carbonate aquifer. *International Journal of Greenhouse Gas Control* 44, 310-322.
56. Wilkin, R.T., DiGiulio, D.C. (2010). Geochemical impacts to groundwater from geologic carbon sequestration: controls on pH and inorganic carbon concentrations from reaction path and kinetic modeling. *Environmental Science & Technology* 44 (12), 4821-4827.

57. Yang, C., Mickler, P. J., Reedy, R., Scanlon, B. R., Romanak, K. D., Nicot, J. P., Hovorka, S. D., Treviño, R.H., Larson, T. (2013). Single-well push-pull test for assessing potential impacts of CO₂ leakage on groundwater quality in a shallow Gulf Coast aquifer in Cranfield, Mississippi. *International Journal of Greenhouse Gas Control* 18, 375-387.
58. Yang, C., Delgado-Alonso, J., Hovorka, S.D., Mickler, P., Trevino, R.H., Phillips, S. (2014a). Monitoring dissolved CO₂ in groundwater for CO₂ leakage detection in aquifer. *Energy Procedia* 63, 4209-4215.
59. Yang, C., Hovorka, S. D., Delgado-Alonso, J., Mickler, P. J., Treviño, R.H., Phillips, S. (2014b). Field demonstration of CO₂ leakage detection in potable aquifers with a pulslike CO₂-release test. *Environmental science and technology*, 48(23), 14031-14040.
60. Zheng, L., Apps, J.A., Spycher, N., Birkholzer, J.T., Kharaka, Y.K., Thordsen, J., Beers, S.R., Herkelrath, W.N., Kakouros, E., Trautz, R.C. (2012). *International Journal of Greenhouse Gas Control* 7, 202-217.
61. Zhu, Q., Li, X., Jiang, Z., Wei, N. (2015). Impacts of CO₂ leakage into shallow formations on groundwater chemistry. *Fuel Processing Technology* 135, 162-167.

Figure 1: Geographical location of the experimental site. **A:** Location of Saint-Emilion in France. **B:** Location of the experimental site in the town of Saint-Emilion.

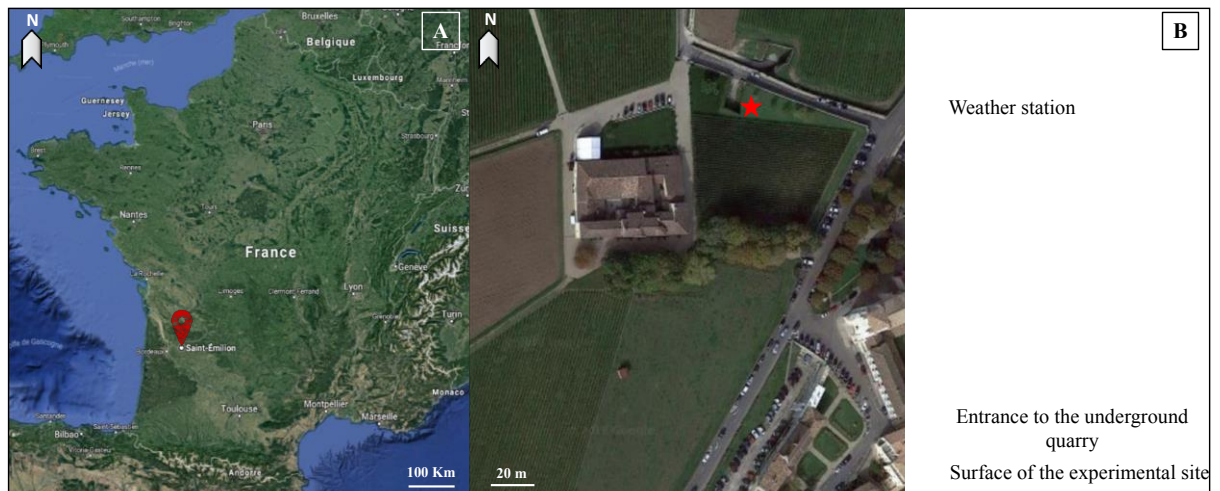
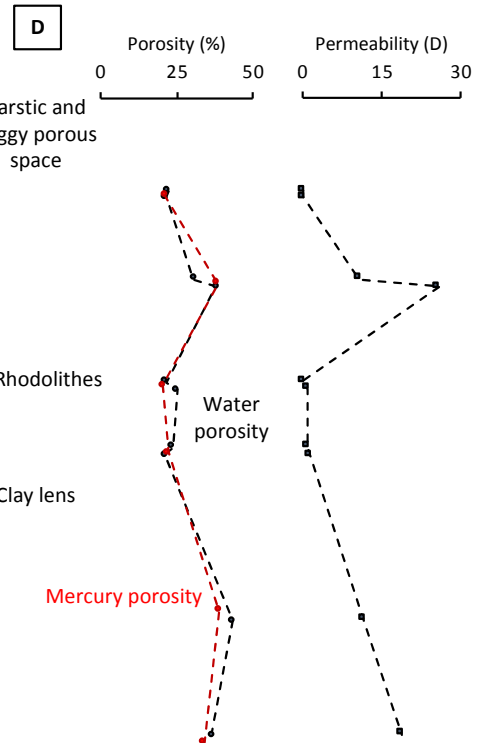
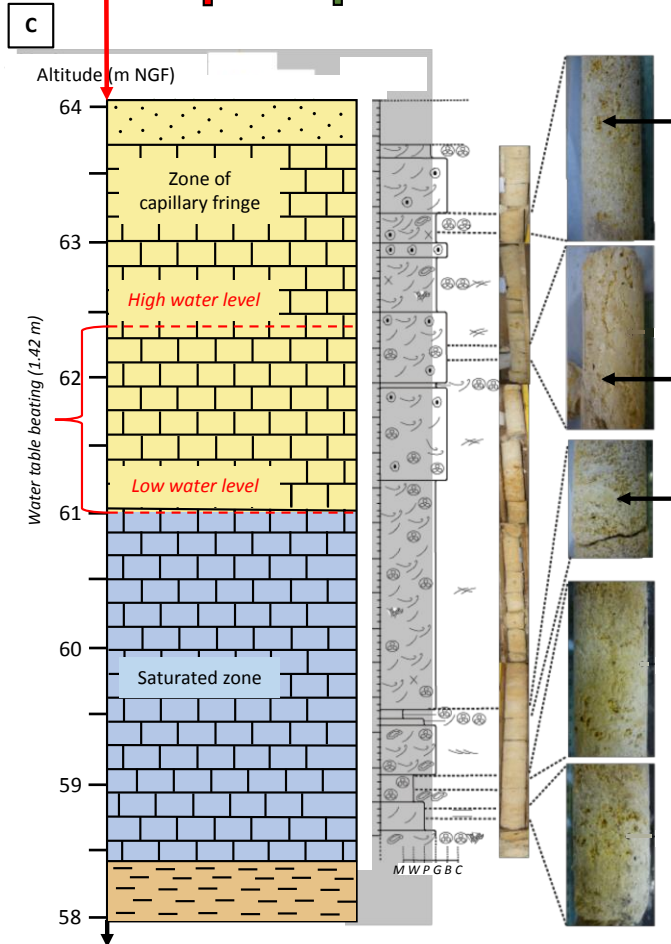
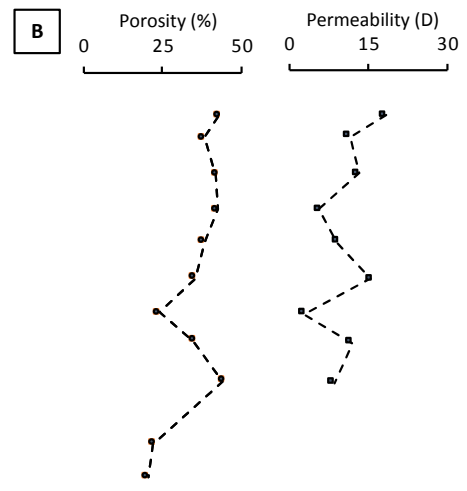
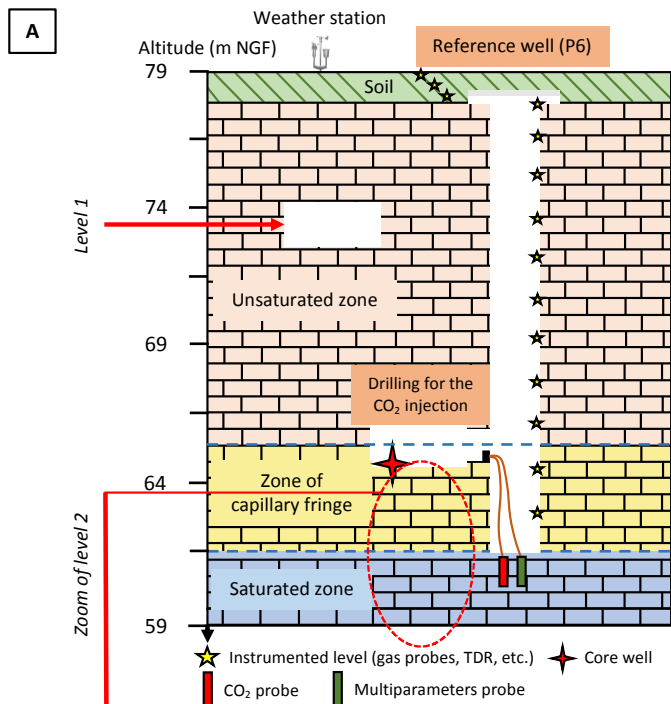


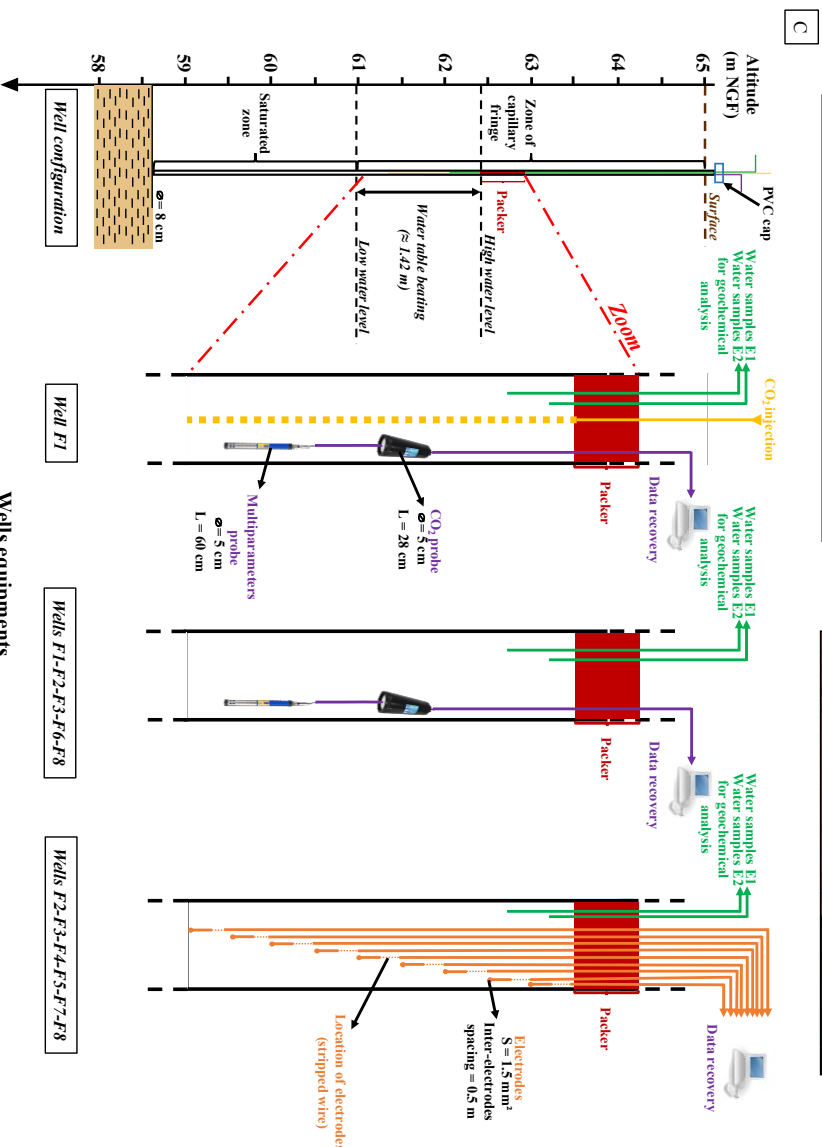
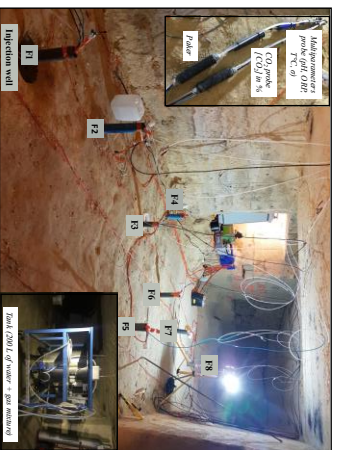
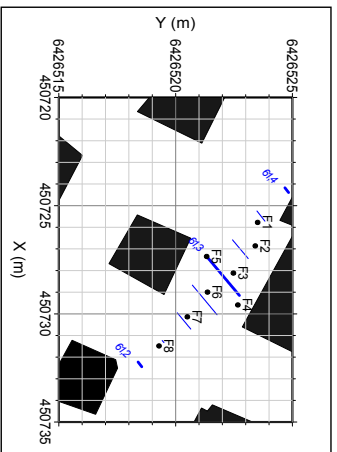
Figure 2: Cross-section of the underground quarry. **A:** Cross-section from the surface to the saturated zone. The reference well P6 is equipped with multiple probes and sensors at different altitudes. The injection and observation wells are located at approximately about 64 m NGF. **B:** Evolution of porosity (%) and permeability (D) from the surface to the aquifer. **C:** Zoom of the figure 2.A. Cross-section of the capillary fringe zone and saturated zone, in the level 2, with the corresponding stratigraphic log and associated facies. **D:** Evolution of porosity (%) and permeability (D) by Hg-injection and variable head air permeameter methods respectively, from 63.5 m to 59.5 m NGF, throughout the capillary fringe and saturated zone.



Legend

Lithologies	Elements	Sedimentary structures
Backfill	Undetermined foraminifers	Straight structure
Limestone	Bioclasts undifferentiated	Oblique structure
Sannoisian marls	Lamellibranchia	Cross-bedded structure
	Oncoids	
	Rhodolithes	
	Bryozoans	
	Echinoderm debris	

Figure 3: Location and equipment of wells. **A:** Level 2 location plan and position of the 8 wells (Lambert II coordinates). The blue dotted lines indicate the isopiestic line of the aquifer in July 8, 2019. The black squares correspond to quarry's pillars. The white background is the surface of the ground. **B:** Level 2 photograph. The wells are numbered from 1 to 8 and are arranged in the direction of flow of the groundwater, F1 being the most upstream well where the CO₂ injection took place. The photograph in the square at the top left shows the multiparameters and CO₂ probes (measuring the physicochemical parameters of the aquifer), arranged in certain wells and immersed in the water table. The photograph in the square at the bottom right shows the tank containing 200 L of water where a gas composed of 90% CO₂, 9% He and 1% Kr have been dissolved and mixed until homogenized before being injected into well F1. **C:** Schematic representation of well equipment, across the capillary fringe and the saturated zones. All boreholes are equipped with packers, allowing the well to be sealed, as well as tubings enabling the recovery of water samples for geochemical analyzes. Well F1 has a supplementary tubing permitting the injection of gas. A multiparameters probe is placed in wells F1, F3, F6, F8. A CO₂ probe is present in wells F1, F2, F3 and F8. These are connected to a computer allowing data recovery. The wells F2, F3, F4, F5, F7 and F8 are additionally equipped with 9 electrodes immersed in the aquifer, making it possible to perform electrical resistivity tomography measurements. These results will be the subject of another study.



Wells equipments

Figure 4: Evolution of electrical conductivity ($\mu\text{S/cm}$) for the wells F1, F2, F3, F4, F6, F7 and F8 after injection of a saline solution (2 g/L) into the well F1 the March 29, 2019. The velocity (m/day) of the injected solution through the carbonate freshwater aquifer is calculated in the table 1.

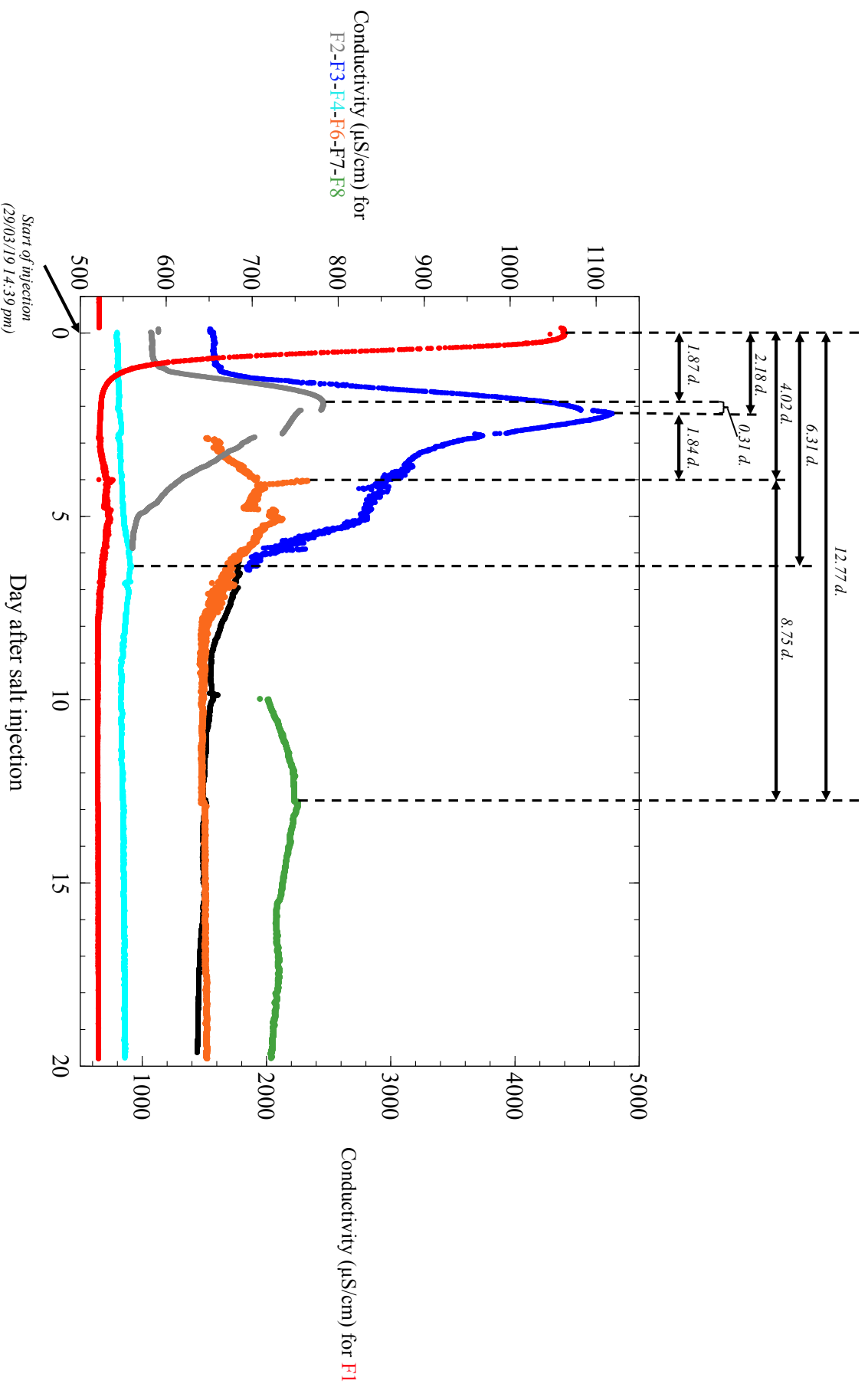
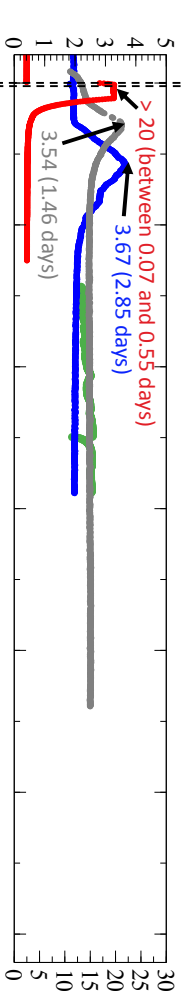


Figure 5. Evolution and comparison of the different physicogeochemical parameters measured by the CO₂ and multiparameter probes for the wells F1, F2, F3, F6 and F8 after CO₂ injection in the well F1 the July 09, 2019 10 am: a) CO₂ concentration ($\pm 5\%$) over time; b) electrical conductivity ($\pm 0.5\%$ of reading plus $1.0\ \mu\text{S}\cdot\text{cm}^{-1}$) over time; c) pH (± 0.1 pH units) over time; and d) ORP (± 5.0 mV) over time. The maximums for each parameter (with value and number of days to reach the maximum value from the date of injection) are indicated, as well as the start and end of the CO₂ injection.

Start of Injection
(09/07 10 am)

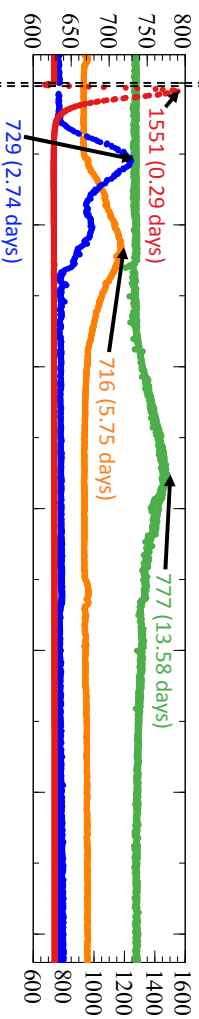
End of Injection
(09/07 11:30 am)

a
CO₂ concentration (%) for F2-F3-F8



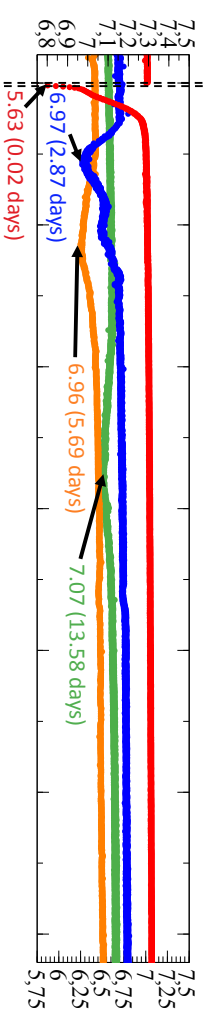
CO₂ concentration (%) for F1

b
Conductivity (μS/cm) for F3-F6-F8



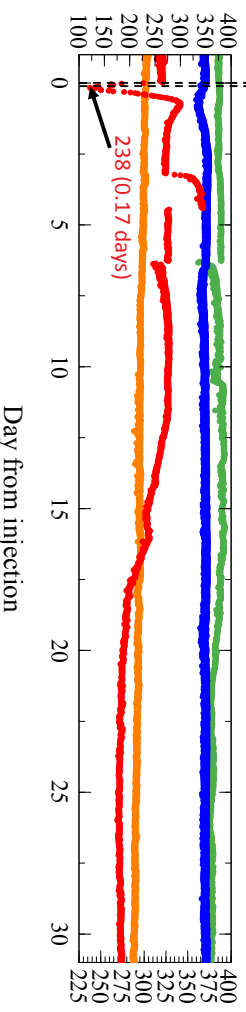
Conductivity (μS/cm) for F1

c
pH for F3-F6-F8



pH for F1

d
ORP (mV) for F3-F6-F8



ORP (mV) for F1

Figure 6: Evolution of Ca^{2+} concentrations (mg/L) from July 4 to 31, 2019 for well F1. The concentrations were obtained at two different depths: E1 (black dots) at 25 cm and E2 (gray dots) at 70 cm below the water table level.

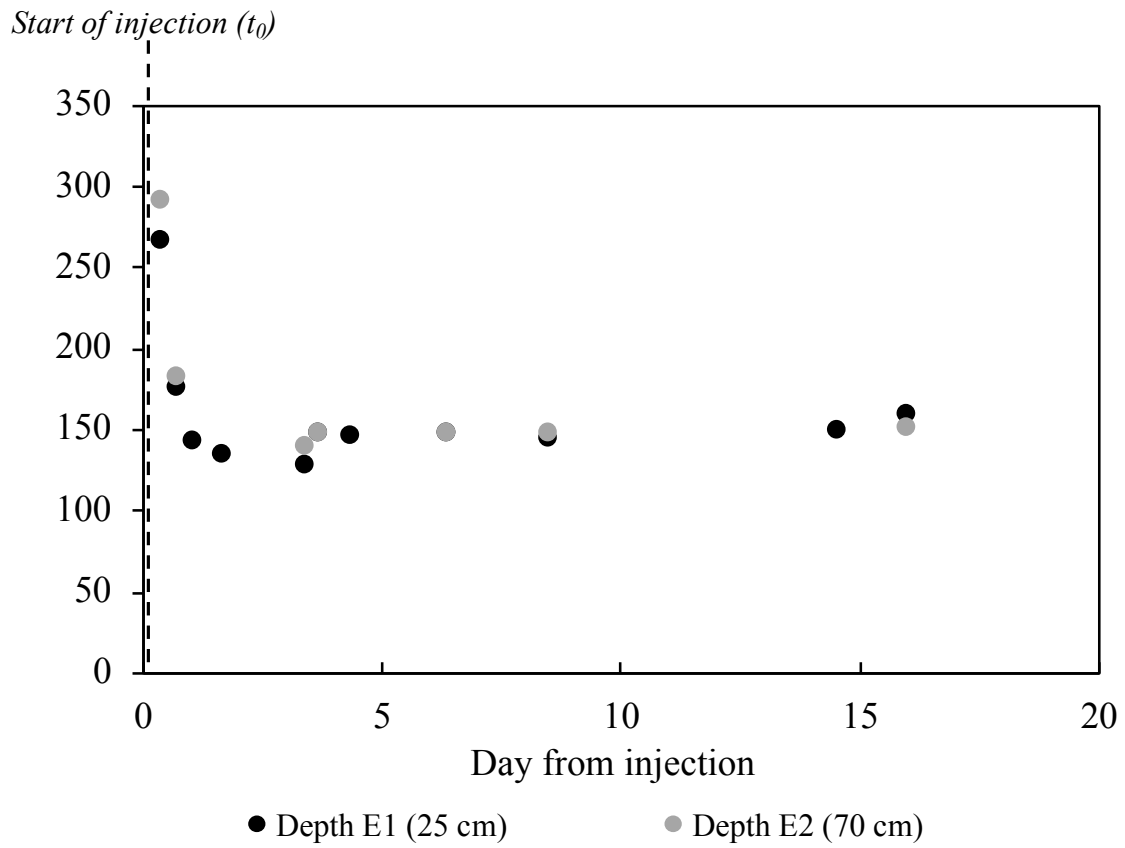


Figure 7: Evolution of the concentrations of the cations and the anions (mg/L) over time for wells F1, F2, F3, F6 and F8, after the CO₂ injection in well F1 the July 09, 2019. The horizontal dotted lines represent the initial concentrations of the different ionic species, measured before the injection of CO₂.

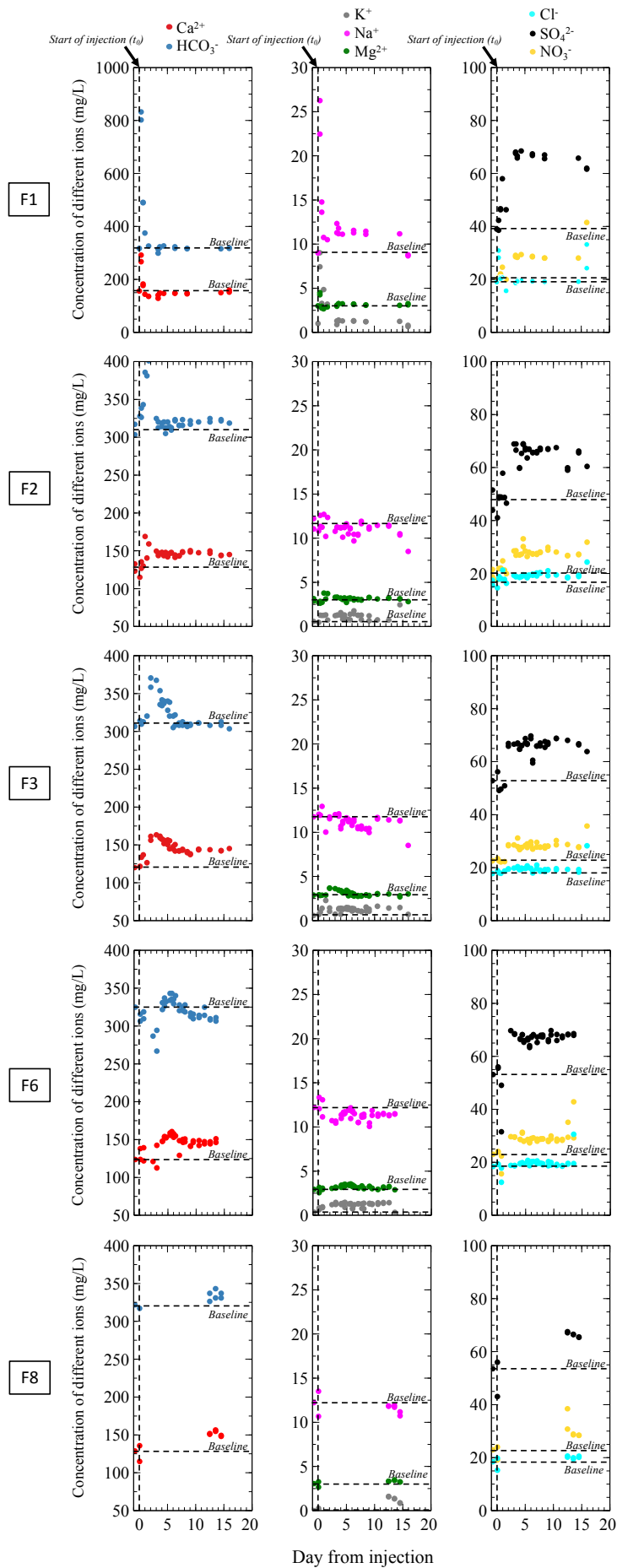


Figure 8: Evolution of the conductivity velocity peak as a function of the distance (in m) from well F1 for NaCl and CO₂ injection (red and black dots respectively); and associated permeability values (in Darcy; green cross).

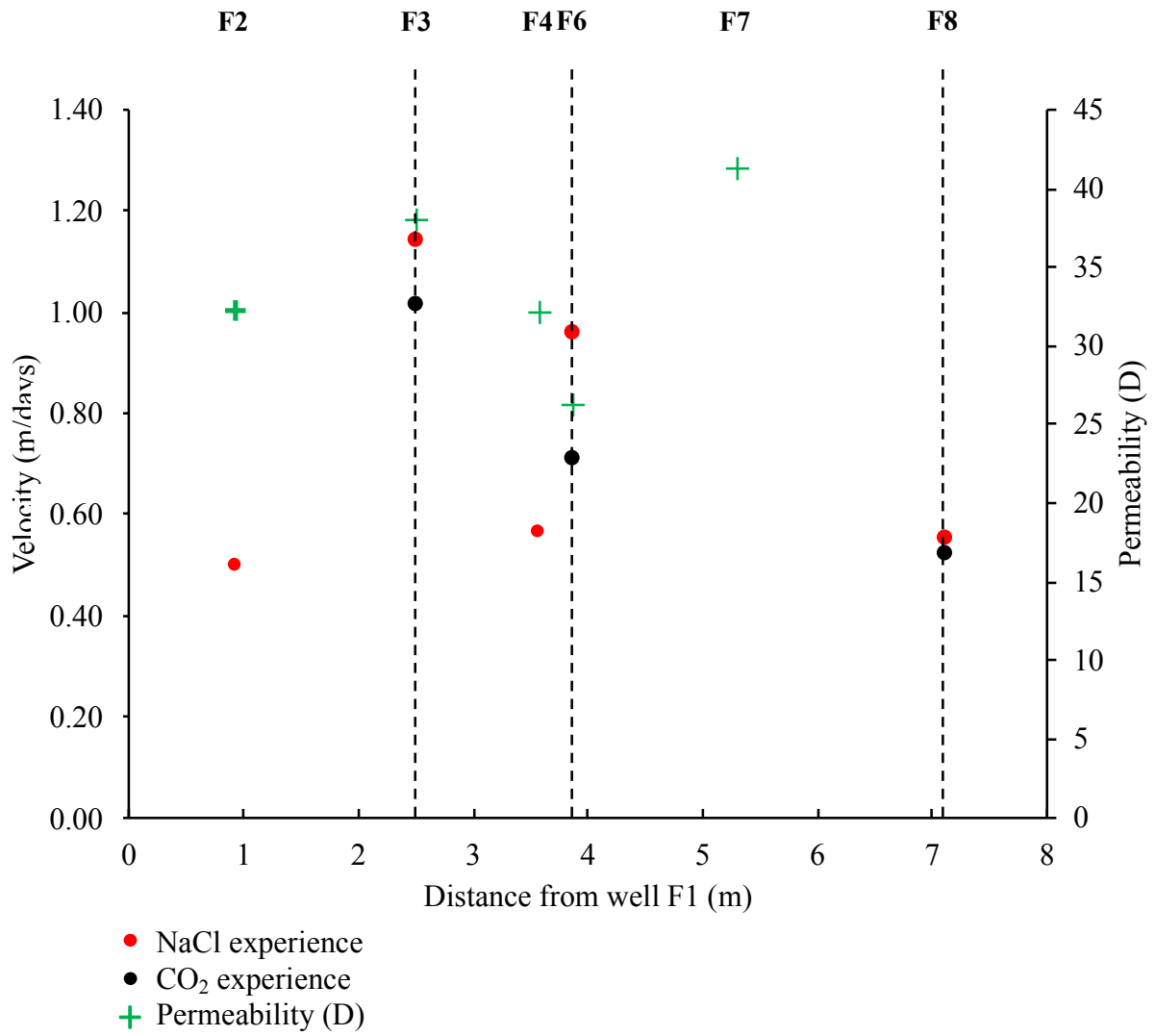


Figure 9: Evolution of the CO₂ concentrations measured by the CO₂ probe (%) immersed in the water table in wells F1, F2, F3 and F8 compared to the concentrations calculated with the PhreeqC software (%) (black crosses) over time. These evolutions are superimposed with the calculation of calcite saturation index (orange crosses) obtained with the same software. The vertical dotted line corresponds to the time of injection (July 09, 2019 at 10 am); the horizontal dotted line indicates the equilibrium zone of the calcite, separating the calcite precipitation and dissolution zone.

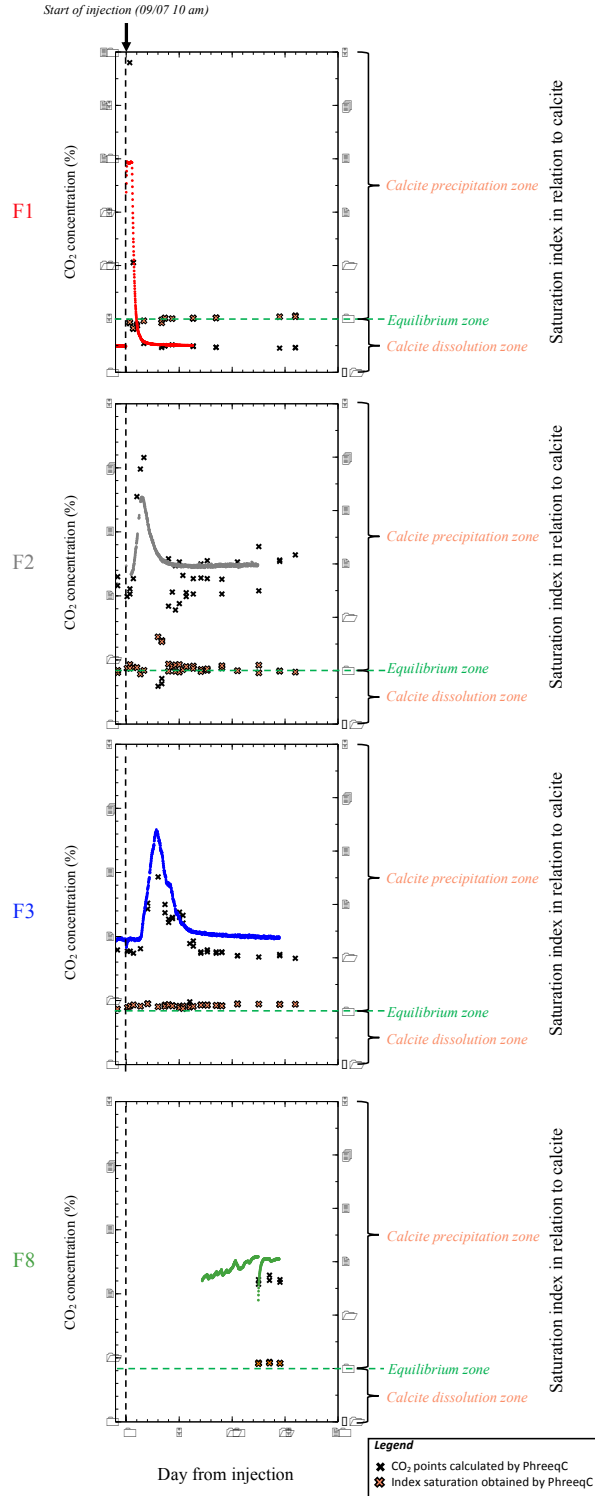
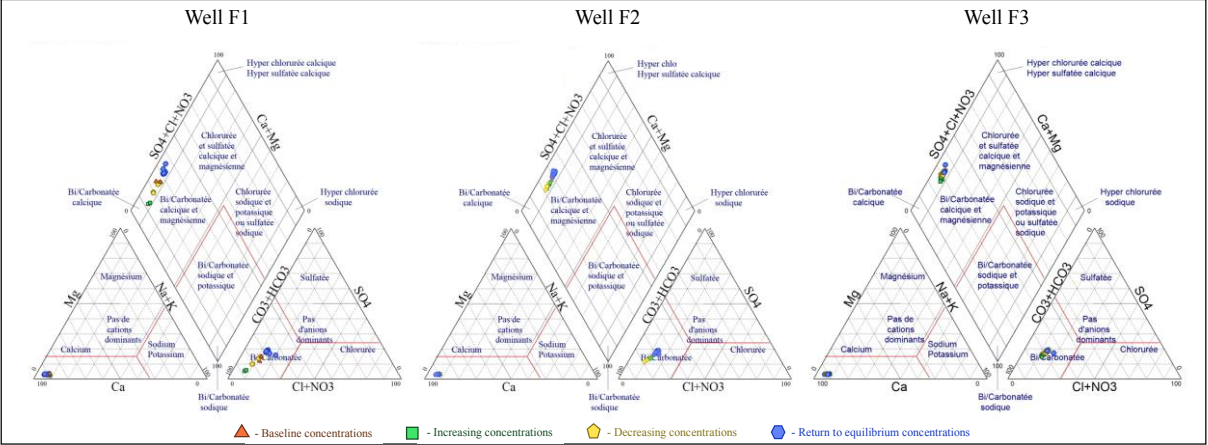


Figure 10: Piper diagram: Evolution of the water facies for wells F1, F2 and F3 before, during and after CO₂ injection. According to the baseline concentrations of cations and anions, the water is initially of calcium and magnesium bi-carbonated type. After injection, the water facies moves toward the bi-carbonated calcium pole. After that, the facies gradually migrate in the opposite direction to the chlorinated-sulphated calcium pole.



AUTHORSHIP STATEMENT

Manuscript title: **Aquifer-CO₂ Leak project: Physicochemical characterization of the CO₂ leakage impact on a carbonate shallow freshwater aquifer**

All persons who meet authorship criteria are listed as authors, and all authors certify that they have participated sufficiently in the work to take public responsibility for the content, including participation in the concept, design, analysis, writing, or revision of the manuscript. Furthermore, each author certifies that this material or similar material has not been and will not be submitted to or published in any other publication before its appearance in the *Hong Kong Journal of Occupational Therapy*.

Authorship contributions

Please indicate the specific contributions made by each author (list the authors' initials followed by their surnames, e.g., Y.L. Cheung). The name of each author must appear at least once in each of the three categories below.

Category 1

Conception and design of study:

A Petit; A. Cerepi, C. Loisy; O. Le Roux; L. Rossi; A. Estublier; J. Gance; B. Garcia; B. Hautefeuille; B. Lavielle; T. Brichart; S. Noirez; F. Martin; B. Texier; S. Kennedy; A. El Khamlichi.

Acquisition of data:

A Petit; A. Cerepi, C. Loisy; O. Le Roux; L. Rossi; A. Estublier; J. Gance; B. Garcia; B. Hautefeuille; B. Lavielle; T. Brichart; S. Noirez ; F. Martin; B. Texier ; S. Kennedy.

analysis and/or interpretation of data A Petit; A. Cerepi, C. Loisy; O. Le Roux; A. Estublier; B. Garcia

Category 2

Drafting the manuscript:

A Petit; A. Cerepi, C. Loisy; O. Le Roux; A. Estublier; B. Garcia ; S. Kennedy.

revising the manuscript critically for important intellectual content:

A Petit; A. Cerepi, C. Loisy; O. Le Roux; A. Estublier; B. Garcia

Category 3

Approval of the version of the manuscript to be published (the names of all authors must be listed):

A Petit; A. Cerepi, C. Loisy; O. Le Roux; L. Rossi; A. Estublier; J. Gance; B. Garcia; B. Hautefeuille; B. Lavielle; T. Brichart; S. Noirez; F. Martin; B. Texier ; S. Kennedy; A. El Khamlichi.